VARIATIONS IN STORM STRUCTURE AND PRECIPITATION CHARACTERISTICS ASSOCIATED WITH THE DEGREE OF ENVIRONMENTAL BAROCLINICITY IN SOUTHEAST TEXAS

A Thesis

by

KAREN ELIZABETH BRUGMAN

Submitted to the Office of Graduate Studies of
Texas A&M University
in partial fulfillment of the requirements for the degree of

MASTER OF SCIENCE

August 2007

Major Subject: Atmospheric Sciences

VARIATIONS IN STORM STRUCTURE AND PRECIPITATION CHARACTERISTICS ASSOCIATED WITH THE DEGREE OF ENVIRONMENTAL BAROCLINICITY IN SOUTHEAST TEXAS

A Thesis

by

KAREN ELIZABETH BRUGMAN

Submitted to the Office of Graduate Studies of
Texas A&M University
in partial fulfillment of the requirements for the degree of

MASTER OF SCIENCE

Approved by:

Chair of Committee,	Courtney Schumacher
Committee Members,	John Nielsen-Gammon
	Steven F. DiMarco
Head of Department,	Richard Orville

August 2007

Major Subject: Atmospheric Sciences

ABSTRACT

Variations in Storm Structure and Precipitation Characteristics Associated with the Degree of Environmental Baroclinicity in Southeast Texas. (August 2007)

Karen Elizabeth Brugman, B.S., University of California, Los Angeles

Chair of Advisory Committee: Dr. Courtney Schumacher

The large-scale environment can have a significant impact on subtropical precipitating systems via the baroclinicity of the environment and the associated dynamical forcings. The degree of baroclinicity is examined using National Centers for Environmental Prediction (NCEP) reanalysis temperature and zonal wind fields over a two-year period for Southeast Texas, yielding classifications of barotropic, weakly baroclinic, and strongly baroclinic for the background environment. Weakly baroclinic environments accounted for half of the days throughout the two-year period. Barotropic environments occurred most frequently during summer and strongly baroclinic environments occurred most frequently in winter, although less often than weakly baroclinic environments.

A climatology of storm types, based on dynamical forcing (i.e., weak forcing, drylines, cold fronts, warm fronts, stationary fronts and upper level disturbances) and precipitation structure (i.e., isolated, scattered, widespread, linear, unorganized and leading-line/trailing stratiform), was compiled and compared to the baroclinicity designations. Non-frontal storm types (i.e., weak forcing, drylines and upper level disturbances) are typical of barotropic environments, while frontal storm types (i.e.,

warm, cold and stationary fronts) are typical of weakly and strongly baroclinic environments.

Storm events and drop-size distributions (DSD) were identified from surface rainfall data collected by a Joss-Waldvogel disdrometer located in College Station, Texas. The DSDs were compared by baroclinicity and storm type. The barotropic DSD is weighted towards the largest drops because of the stronger convection and stratiform precipitation in the weak forcing and dryline storm types, while the strongly baroclinic DSD is weighted towards the smallest drops because of the weaker convection from the warm fronts and stationary fronts. The weakly baroclinic DSD is weighted more evenly towards small and large drops than the barotropic and strongly baroclinic DSDs because of the conflicting microphysical processes in the different storm types. The microphysical processes within the storms vary by storm type and baroclinicity regime, such that the large-scale environment modifies the precipitation characteristics of storms in SE Texas.

NOMENCLATURE

B	Barotropic
DJF	December, January, February
DSD	Drop-size distribution
JJA	June, July, August
JW	Joss-Waldvogel
MAM	March, April, May
MCS	Mesoscale convective system
NCEP	National Centers for Environmental Prediction
R	Rain rate
RA	Rain accumulation
W	Weakly Baroclinic
S	Strongly Baroclinic
SON	September, October, November
Z	Radar reflectivity factor

TABLE OF CONTENTS

LIST OF FIGURES

FIGURE Page

FIGURE Page

LIST OF TABLES

TABLE Page

1. INTRODUCTION

1.1. Baroclinicity and the Subtropics

Global circulations work to reduce meridional temperature differences. The subtropics act as a transition zone between the midlatitude and tropical regimes. Barotropic environments in the subtropics represent tropical influences while baroclinic environments represent midlatitude influences. An understanding of environmental baroclinicity and the global circulation is necessary to evaluate the complex interactions between the tropics, subtropics and midlatitudes.

Differential heating of the earth by solar radiation drives global circulations. The thermally direct Hadley Cell is the primary mechanism for transporting tropical heat and energy to the subtropics. In the mid-latitudes, however, energy transport is primarily due to transient baroclinic eddies, which transport heat from the subtropics to higher latitudes (Trenberth and Stepaniak 2003). Subsidence in the Hadley circulation occurs in the subtropics where tropical air descends to the surface near the subtropical highs. Trenberth and Stepaniak (2003) concluded that clear sky radiative cooling and advection cooling by transient eddies balance the adiabatic compression warming in the subsiding branch of the Hadley circulation.

The extent and strength of the Hadley circulation is highly coupled to the seasonal cycle. The shift in the latitude of maximum heating across the equator to the

---

This thesis follows the style of the *Journal of the Atmospheric Sciences.*

summer hemisphere results in a decrease (increase) in the strength and extent of the summer (winter) hemisphere Hadley circulations (Fig. 1). Hou (1998) concluded that with a stronger Hadley cell, there has to be more transport out of the tropics, which also increases the heat transport by transient eddies towards the poles. Cook (2003) showed that in the winter hemisphere stronger vertical wind shear in the descending branch increases surface friction, which is balanced by the Coriolis force, thereby increasing the strength of the Hadley circulation. However, in the summer hemisphere a decrease in the momentum flux in the descending branch of the Hadley circulation due to anomalous lows associated with the summer monsoons decrease the subtropical highs, which lessens the meridional pressure gradients and the Hadley circulation (Cook 2003).

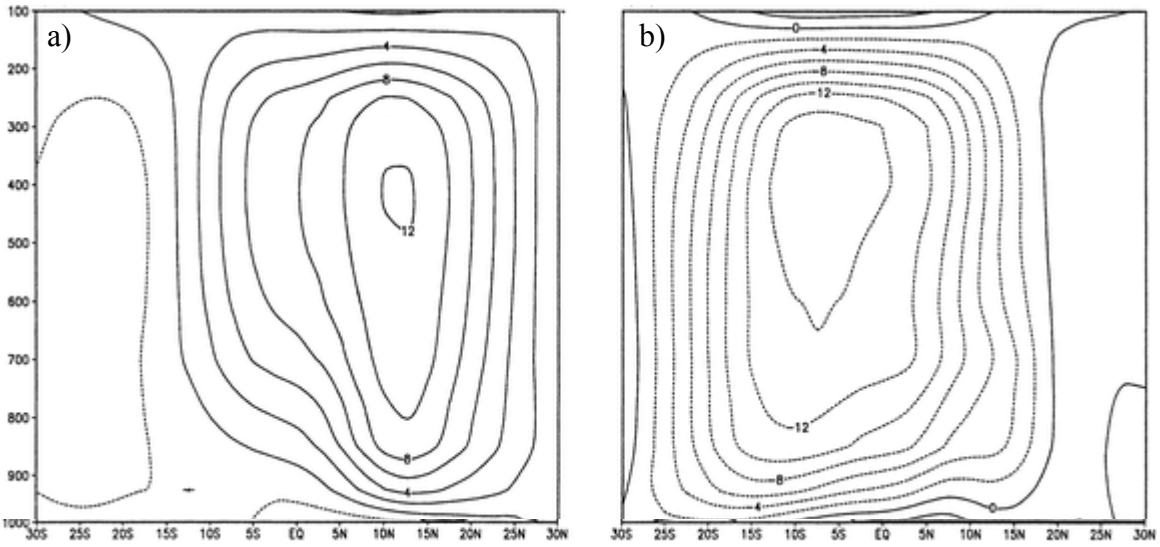

Figure 1 Monthly mean Stokes streamfunction from NCEP reanalysis climatology for a) January and b) July. Streamlines represent rising motions near the equator and sinking motions at higher latitudes (from Cook 2003).

1.1.1. Barotropic Environment

Holton (1992) defines a barotropic atmosphere as one in which density is only a function of pressure. This relationship indicates that surfaces of constant density are surfaces of constant pressure, and therefore by the ideal gas law also surfaces of constant temperature. Using the thermal wind equation to relate the horizontal temperature gradient and the vertical shear of the geostrophic wind, Wallace and Hobbs (1977) showed that in a barotropic atmosphere there is no vertical shear of the geostrophic wind and little or no temperature advection. Therefore, in a pure barotropic environment pressure surfaces will be vertically stacked and the direction and speed of the geostrophic wind is independent of height (Holton 1992, Wallace and Hobbs 1977).

In addition, Wallace and Hobbs (1977) maintain that there exist regions where the thickness and height contours are parallel in the presence of horizontal temperature gradients, which can be defined as equivalent barotropic atmospheres. In these regions, only the direction of the geostrophic wind is independent of height, while the speed varies with height. The change in the magnitude of the geostrophic wind vector is due to variations in the slope of the pressure surfaces with height.

Barotropic conditions are climatologically prevalent in the tropics since there is smaller horizontal temperature variation than at higher latitudes. In the midlatitudes, barotropic conditions are less common but do exist in the absence of frontal systems. The strength and southern penetration of Northern Hemisphere midlatitude cyclones decrease in the summer months, thereby increasing the likelihood of a barotropic

atmosphere. However, the tropics rarely have zero horizontal temperature gradients although they are still considered barotropic.

1.1.2. Baroclinic Environment

As discussed in the previous section, lines of constant height, thickness and temperature are all parallel in a barotropic environment; however, in a baroclinic environment, lines of constant height and thickness intersect such that the geostrophic wind flows across the isotherms instead of purely parallel (Wallace and Hobbs 1977). Holton (1992) showed that surfaces of constant height and thickness are not coincident because density depends upon temperature and pressure in a baroclinic atmosphere. The geostrophic wind inferred from the thermal wind relationship is characterized by vertical shear due to the horizontal temperature gradient. Both the direction and speed of the geostrophic wind will vary with height since the spacing of the height contours varies between pressure levels. The direction of vertical wind shear determines the type of temperature advection in the baroclinic region. Backing of the geostrophic wind is associated with cold temperature advection whereas veering geostrophic winds is associated with warm temperature advection (Wallace and Hobbs 1977).

Baroclinic environments prevail in the midlatitudes where synoptic scale disturbances in the mean flow propagate zonally across the globe. Strong extratropical cyclones or low pressure centers are characterized by closely packed height contours with frontal zones separating regions of warm and cold temperature. As the temperatures

and prevailing winds on either side of the fronts can vary greatly, the baroclinicity of the regions is important to the development of precipitating systems.

1.2. Precipitating Systems

1.2.1. Thunderstorms and MCSs

Single-cell thunderstorms are common in the tropics and occur frequently in the central and southeast portions of the United States, especially during summer, and are the building blocks of other storm types. Byers and Braham (1949) characterize a single-cell thunderstorm as a series of individual convective cells that form in a warm, moist, unstable environment with little vertical wind shear. In these storms, initially strong updrafts keep hydrometeors aloft allowing for the increased growth of precipitation particles, including hail. However, evaporative cooling due to entrainment of drier air increases the downdraft beneath the convective cell as precipitation falls to the ground. Eventually, the downdraft reduces the updraft and the storm decays (Wallace and Hobbs 1977). These storms are usually short lived and can be severe, but lack the organization of multicell and supercell storms.

The presence of wind shear in a warm, moist environment allows for increased organization of thunderstorms. Multicell thunderstorms in the midlatitudes are often associated with frontal boundaries or drylines, which provide surface convergence and vertical wind shear (Houghton 1968, Schaefer 1974). Convective cells form on the leading edge of the storm and mature and decay while new cells continually form. The vertical shear tilts the updrafts and downdrafts such that the development of downdrafts

in the convective region does not suppress the updraft. Dye et al. (1974) showed that the growth of ice particles is primarily by accretion and riming leading eventually to graupel and hail.

A small number of multicell storms will organize into supercell storms when the individual cells merge into a single, highly organized cell (Wallace and Hobbs 1977). Supercells are prevalent in the central US, but are rare in the tropics unless they are associated with a tropical cyclone. Multicell thunderstorms can also organize into squall lines, which have a leading line of convective cells perpendicular to the propagation direction of the storm. Many mature squall lines also include a trailing stratiform region downstream of the environmental shear. The outflow from a squall line downdraft can form a gust front ahead of the convective line, producing strong winds (Wallace and Hobbs 1977).

Squall lines and other convective storms of large horizontal extent (i.e., with precipitation approximately 100 km in one direction) are defined by Houze (1993, 2004) as mesoscale convective systems (MCS), and can be found in both the tropics and midlatitudes. A pattern of convective and mesoscale updrafts and downdrafts comprise the basic structure of the storms. When deep convection initiates within the developing MCS, the formation of a trailing stratiform region follows, although MCSs are often messy without a leading line-trailing stratiform structure (Houze 2004). Figure 2 shows a schematic of an MCS.

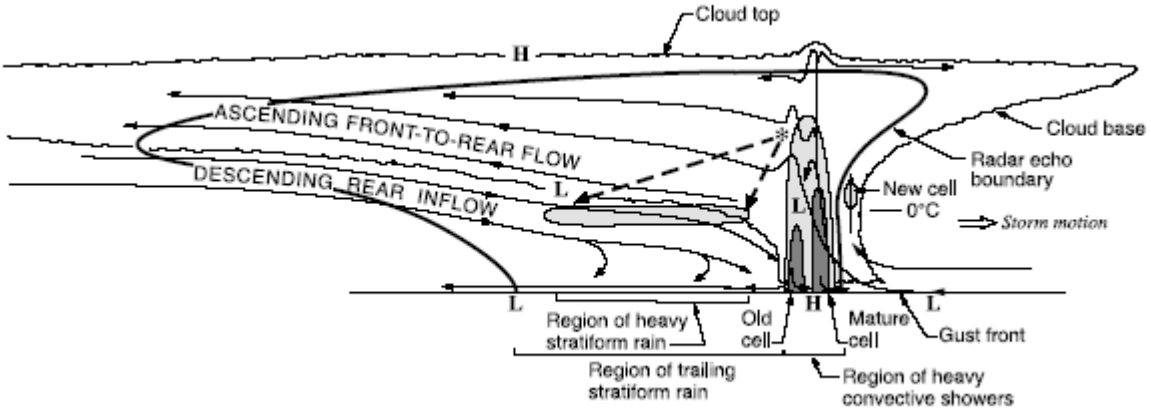

Figure 2 Schematic of MCS (from Houze 2004).

1.2.2. Tropical Cloud Clusters

Convective cloud clusters dominate the precipitation in the tropics. The structure and extent of the clusters varies from individual, shallow convective cells to organized MCSs (Houze 1977, 1981, 1989, Schumacher and Houze 2003a,b, Zipser 2003). Although MCSs are larger and more organized, isolated convective cells are also important because they account for a large percent of rain in tropical regions outside of the rainy regions (Schumacher and Houze 2003b). Zipser (2003) described the possible sources of mesoscale organization of tropical rainfall, including orography, land-sea variations and synoptic scale waves. Organization can be in the form of squall lines or non-squall clusters. The characteristics of tropical precipitating systems show significant seasonal, diurnal and land/ocean variations. Schumacher and Houze (2003a) and Nesbitt et al. (2003) used radar data from the Tropical Rainfall Measurement Mission (TRMM) satellite to produce a climatology of tropical precipitation. They found that continental regions show a more pronounced diurnal and seasonal cycle than ocean regions, and that

while convection is strongest over land, the ocean systems have more robust stratiform regions.

1.2.3. Extratropical Cyclones

Extratropical cyclones consist of a low pressure center with a pair of fronts separating the warm and cold sectors (Fig. 3). The structure and scale of the individual features can vary greatly depending on the large-scale environment and have been studied extensively due to their importance to midlatitude weather (e.g. Matejka et al. 1980, Hobbs et al. 1980, Houze et al. 1981). Matejka et al. (1980) demonstrated that the density differences between the warm and cold sectors leads to ascent along the frontal boundaries.

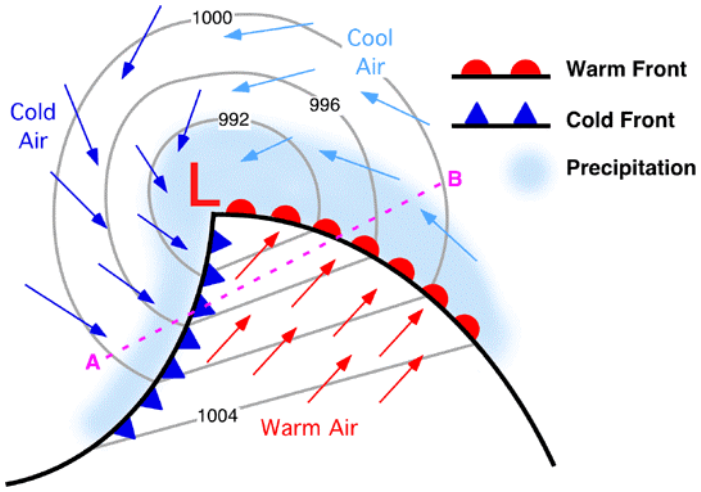

Figure 3 Schematic of extratropical cyclone structure (from Encyclopedia of Earth, June 2007).

Precipitation in the vicinity of the fronts is common, but the structure and type of precipitation varies between the warm and cold fronts. Matejka et al. (1980) studied the structure of warm and cold frontal rainbands, noting that lifting over warm fronts is gentler and covers a larger horizontal extent than cold fronts such that the warm frontal precipitation is generally non-convective, widespread and occurs primarily ahead of the frontal boundary.

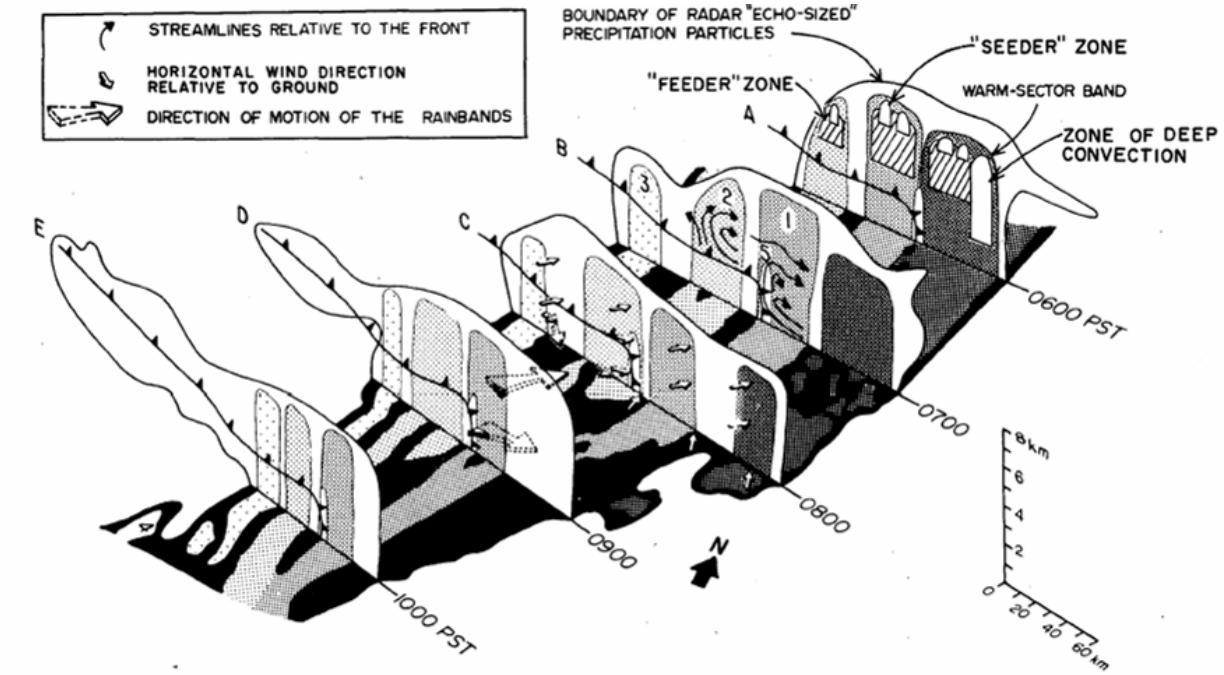

Figure 4 Schematic of rainbands associated with a cold front (from Hobbs et al. 1980).

Hobbs et al. (1980) describe three precipitation structures associated with the cold front (Fig. 4). Ahead of the cold front, warm sector rainbands form near the surface front, with new convective structures developing at the leading edge of the rainband and older convective cells becoming more stratiform in nature. Rainbands along the surface

frontal boundary often have convective towers along the leading edge associated with surface convergence driving strong updrafts. Behind the cold front, rainbands are primarily non-convective and associated with frontal lifting along the upper boundary of the frontal zone. The manner in which precipitation varies between these different storm types can be studied using measurements of surface rainfall parameters.

1.3. Precipitation Characteristics

1.3.1. Drop-Size Distributions

The precipitation from storm systems is not composed of droplets all identical in size and consistent from storm to storm. Instead, precipitation is a selection of drops varying across all or some of the possible range of drop-sizes, from very small to large drops. The drop-size distribution (DSD) of a sample is defined by measuring the number of drops as a function of drop diameter in a certain time interval and place (Jameson and Kostinski 2001). Many properties of rainfall, such as rain rate (R), radar reflectivity factor (Z), and liquid water content (W) can be determined from the DSD of a drop sample. Variations in the DSD and calculated parameters yield valuable insight into the microphysical origins of the rain within the clouds.

Measurements of drop-size distributions can be made using several different instruments. One of the first DSD collection methods was created by Marshall and Palmer (1948), who recorded drops at the ground by impacts on filter paper. An electronic method was developed by Joss and Waldvogel (1967) with the invention of the disdrometer, which converts mechanical drop impacts into electrical signals that are

then processed into DSDs. Other instruments that measure DSDs include optical probes flown on aircraft, video disdrometers, and vertically pointing wind profilers. Once the data has been collected, the DSDs can be compared using a statistical parameterization.

1.3.2. DSD Parameterization

Exponential and gamma distributions are used to parameterize the DSD. The exponential distribution was first used to approximate the DSD by Marshall and Palmer (1948), such that

$$N(D) = N_0 e^{-\Lambda D} \quad , \qquad [1]$$

where N(D) is the number concentration of drops with a given diameter D (mm) in a volume (m^3) of air with units $m^{-3}mm^{-1}$. N_0 is the number concentration of drops and can be calculated using the DSD, while Λ is the slope of the exponential distribution. More recently, Ulbrich (1983) used the gamma distribution (Eq. 2) in place of the exponential distribution since the gamma distribution captures the observed decrease of the DSD for very small drops.

$$N(D) = N_0 D^{\mu} e^{-\Lambda D} \qquad [2]$$

The exponential distribution is therefore a special case of the gamma distribution where the shape parameter μ is set to zero. Since the exponential distribution contains one less

free variable than the gamma distribution, it is often used in place of the gamma distribution for ease of calculations; however, empirical relationships between the shape and slope parameters have been derived to simplify the gamma distribution (Seifert 2005).

N_0 and Λ can be calculated from the moments of the measured drop-size distribution (Waldvogel 1974). Given the number of drops of a given diameter in a time interval, the liquid water content W (Eq. 3), and the radar reflectivity factor Z (Eq. 4), are calculated from the exponential distribution.

$$W = \frac{\pi}{6}\int_0^\infty N(D)D^3 dD \qquad [3]$$

$$Z = \int_0^\infty N(D)D^6 dD \qquad [4]$$

Equations for N_0 (Eq. 5) and Λ (Eq. 6) are found using the ratio of W to Z.

$$N_o = \frac{1}{\pi}\left(\frac{6!}{\pi}\right)^{4/3}\left(\frac{W}{Z}\right)^{4/3} W \qquad [5]$$

$$\Lambda = \left(\frac{6!}{\pi}\right)^{1/3}\left(\frac{W}{Z}\right)^{1/3} \qquad [6]$$

Variations in these parameters are used to compare DSD characteristics across any precipitation regime. Rain rate can also be calculated directly from the drop-size distribution,

$$R = 6\pi \int_0^\infty N(D) D^3 v(D) dD \quad , \qquad [7]$$

where v(D) is the terminal fall velocity of a drop of diameter D, which has its own set of equations and assumptions based on the balance of drag, buoyant and gravitational forces on a rain drop.

Cumulative raindrop-size distributions evolve into an equilibrium distribution over time. Observations from Joss-Waldvogel (JW) disdrometers and numerical simulations display a tendency towards multimodal distributions with peaks representing different microphysical drop formation processes (List and McFarquhar 1990). However, subsequent research into JW disdrometer data has revealed that strength of multimodal signals in the data can be the result of calibration errors and that the actual equilibrium distributions are unimodal and can be fit to an exponential or gamma distribution (Sheppard 1990, McFarquhar and List 1993, Uijlenhoet et al. 2003, McFarquhar 2004). Once equilibrium has been reached, the median volume diameter for the DSD becomes constant and the multiplicative factor, *b*, in the Z-R relationship (see next section) approaches 1, suggesting that the reflectivity and rain rate parameters are proportional (Uijlenhoet et al. 2003). Furthermore, since a large number of drops are

required to reach a state of equilibrium, the higher the concentration of drops in the rainfall, the faster the DSDs will move toward the equilibrium distribution.

1.3.3. Z-R Relationships

Since disdrometers measure the DSD directly, R and Z can both be calculated explicitly. Scanning radars do not measure the DSD, but instead calculate Z from the measured return signal. Therefore in order to retrieve rain rate from the radar, a Z-R relationship must be used to infer rain rate from the measured radar reflectivity factor. The Z-R relationship is expressed as a power law of the form

$$Z = aR^b \qquad [8]$$

The coefficients can be calculated by transforming the variables into logarithmic space (Atlas 1990, Steiner and Smith 2000) where y = log Z and x = log R. In logarithmic space, Equation 8 can be written as

$$y = \alpha + \beta x \qquad [9]$$

Parameters α and β are calculated through linear regression and returned to linear space such that $\alpha = \log(a)$ and $\beta = b$. In some cases, a fixed, climatologically determined b is used to limit the variability of the multiplicative factor a (Joss and Waldvogel 1969).

Steiner and Smith (2000) calculated the coefficient, *b*, from disdrometer data and found that characteristic values range from 1 – 1.8. Also, Sempere Torres et al. (1994) suggest that the difference between *b* and 1 reflects the departure of the DSD from equilibrium. Greater variability in the multiplicative factor, *a*, than in *b* was observed by Steiner and Smith (2000), which suggests that the development of separate relationships with *a* varying would lead to better rainfall estimation. There have been many studies investigating the variation of Z-R relationships within storms and different precipitations regimes, such as between convective and stratiform, tropical and mid-latitude, or continental and maritime precipitation (Joss and Waldvogel 1970, Waldvogel 1974, Tokay and Short 1996, Steiner and Smith 2000, Steiner et al. 2004). As a result, different Z-R relationships are often applied based for different precipitation regimes.-

1.3.4. Precipitation Microphysics

Precipitation is often classified as either convective or stratiform (Houze 1981, 1997, Steiner and Smith 1998). However, due to the confusion between non-convective stratiform precipitation associated with weak, large-scale lifting and stratiform precipitation from aging convection, it is easier to describe three types of precipitation: convective, stratiform and non-convective.

Convective cells are dominated by strong updrafts that lift precipitation particles formed at the cloud base to upper levels within the convective core (Houze 1989). Water particles grow by collision-coalescence and ice particles grow by accretion and riming. The particles fall toward the ground once they are heavy enough to overcome the

strength of the updraft. In the presence of deep convection in both the midlatitudes and the tropics, hydrometeors may remain at upper levels as the convection decays. These old convective cells merge to form the stratiform region where weak updrafts allow growth of ice particles by vapor diffusion (Rutledge and Houze 1987, Houze 1989). Steiner and Smith (1998) show that as the particles fall towards the melting level, further growth can occur by aggregation.

In the non-convective case, weak vertical air motions, often associated with fronts, lead to widespread precipitation. While convective cells may be embedded in the systems, the dominant microphysical processes are more stratiform in nature with weak frontal lifting leading to ice formation at upper levels by vapor deposition with aggregates forming as the particles fall toward the melting level (Houze et al. 1981, Matejka et al. 1980).

Isolating the microphysical processes that yield particular drop-size distributions has also been a matter of study. Waldvogel (1974) was the first to suggest a relationship between the value of N_0 and the type of precipitation observed. DSDs weighted towards larger drops tend to have smaller values of N_0, while larger values of N_0 represent DSDs weighted towards smaller drops. Widespread rain tends to have moderate values of N_0 (Fig. 5). Waldvogel (1974) observed shifts in the type of precipitation by comparing values of N_0 in a time series. A sudden jump in N_0 corresponded to changes in rain rate and calculated Z-R relationships.

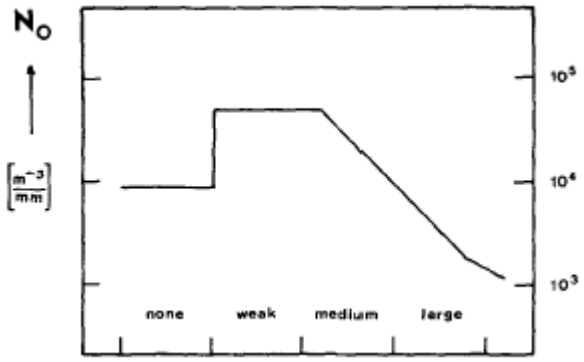

Figure 5 Comparison of N_0 values by strength of convection (from Waldvogel 1974).

Tokay and Short (1996) compared DSDs of convective and stratiform precipitation at the same rain rate. The convective DSDs had more smaller drops and less large drops than the stratiform DSDs. They also found that within the convective DSDs there were varying values of N_0. Medium convection showed the highest values of N_0, whereas non-convective rain showed the lowest values. For moderate rain rates that could be either convective or stratiform, a lower value of N_0 would separate convective from stratiform precipitation in the absence of radar data. Comparing the rainfall parameters by baroclinicity could yield valuable information on the importance of the different types of precipitation within the different categories.

2. METHODS

2.1. Baroclinicity

2.1.1. NCEP Data

The degree of environmental baroclinicity is determined using National Centers for Environmental Prediction (NCEP) reanalysis data for a two-year period from December 2004 through November 2006. The temperature and wind data were evaluated over a 10x10 degree grid box centered over SE Texas (25ºN-35ºN and 100ºW-90ºW) with a resolution of 2.5 degrees.

The horizontal temperature gradient is calculated using NCEP daily mean temperature values taken at 850mb. A fast fourier transform filter was applied to each 2.5 degree grid box over the two-year period to isolate the daily temperature variations. Figure 6 shows an example of the filter applied to one grid box in 2005. It shows the NCEP daily mean temperatures for each day and the resulting daily temperature anomalies used for the subsequent baroclinicity calculations. This filter is much more stringent than simply removing the seasonal cycle, since I was interested in relative baroclinicity variations from day to day. Therefore, baroclinicity in this thesis is meant to indicate relative daily changes rather than absolutely barotropic or baroclinic environments.

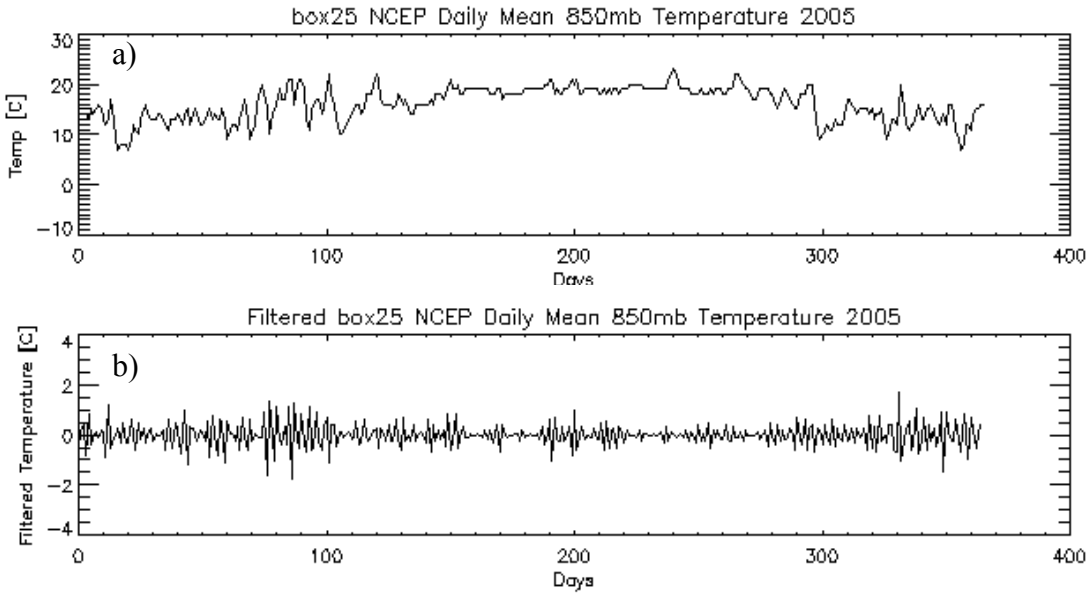

Figure 6 Application of filter on NCEP daily mean 850mb temperature data for a single grid box in 2005 a) original unfiltered data b) filtered data isolating the daily variations.

The maximum temperature difference between the individual boxes across the entire grid was used to calculate the horizontal temperature difference. The larger the maximum temperature difference, the greater the degree of environmental baroclinicity. Maximum temperature differences were calculated using no filter, using a filter to take out the seasonal cycle and the current filter that leaves in only day-to-day variability. The time series had correlations near 0.7, which suggests that while details of the following analysis will vary based on the filter, the overall results will not be as sensitive. In a purely geostrophic atmosphere, the vertical wind shear could be directly inferred from the horizontal temperature gradient using the thermal wind relation. Since

the environment is complicated by other forces, we need to calculate the wind shear independently of the temperature gradient.

Zonal winds are taken over the NCEP grid at 6 pressure levels (850, 700, 600, 500, 400, and 300mb). Winds were taken at and above 850mb to remove boundary layer influences at and below 300mb to minimize the climatological influence of the subtropical jet stream (Fig. 7a). Each grid box was filtered at each pressure level to isolate the daily variations using the same filter used for the temperatures. The filtered zonal wind values at each individual pressure level were averaged across all grid boxes, yielding a single wind value for each pressure level for each day. The maximum wind speed difference between the individual pressure levels within a grid box was used to calculate the vertical wind shear. No differentiation was made between negative or positive values of shear; however, it would be possible to investigate this in future work.

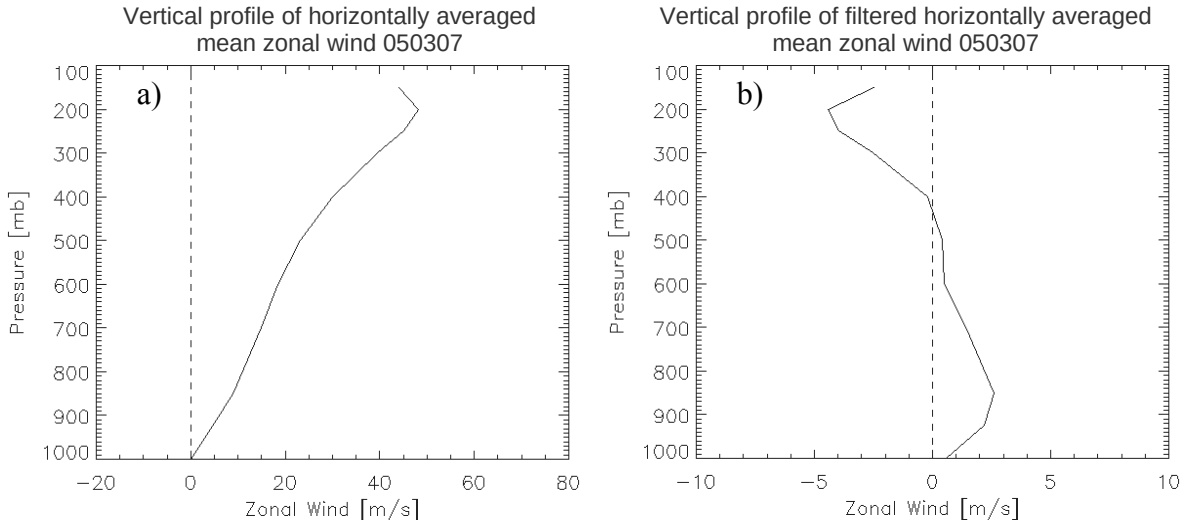

Figure 7 Application of filter on NCEP daily mean zonal wind data. a) Unfiltered vertical distribution of zonal wind with height for single grid box and b) filtered result.

2.1.2. Baroclinicity Designations

The three baroclinicity designations -- barotropic, weakly baroclinic, and strongly baroclinic -- evolved throughout the research. Originally, separate designations for temperature and wind were created arbitrarily and then adjusted based on analysis of the synoptic conditions that contributed to the relative environmental baroclinicity. However, when the temperature and wind designations disagreed there was not a clear method for determining which designation should be weighted more heavily. A single designation for baroclinicity was created that uses both the temperature and wind information equally. Figure 8 is the resulting linear phase-space diagram used to classify the degree of environmental baroclinicity based on day-to-day variations. Each point represents a daily value regardless of whether there was rain in SE Texas.

Three baroclinicity designations were isolated in the central portions of the chart (Fig. 8). Any points outside of these three regions were not used in the analysis because the temperature and wind designations differed by such an extent that a single designation loses vital information about the synoptic conditions. The center line represents thermal wind balance. The slope of the crossbars separating the three classes is the 3:2 ratio of scale of the temperature to the wind designations, and the actual position of the crossbars were dynamically determined by examining storm clusters (see Sec. 2.3.3.) along boundaries to insure that similar storms were not separated into different classes.

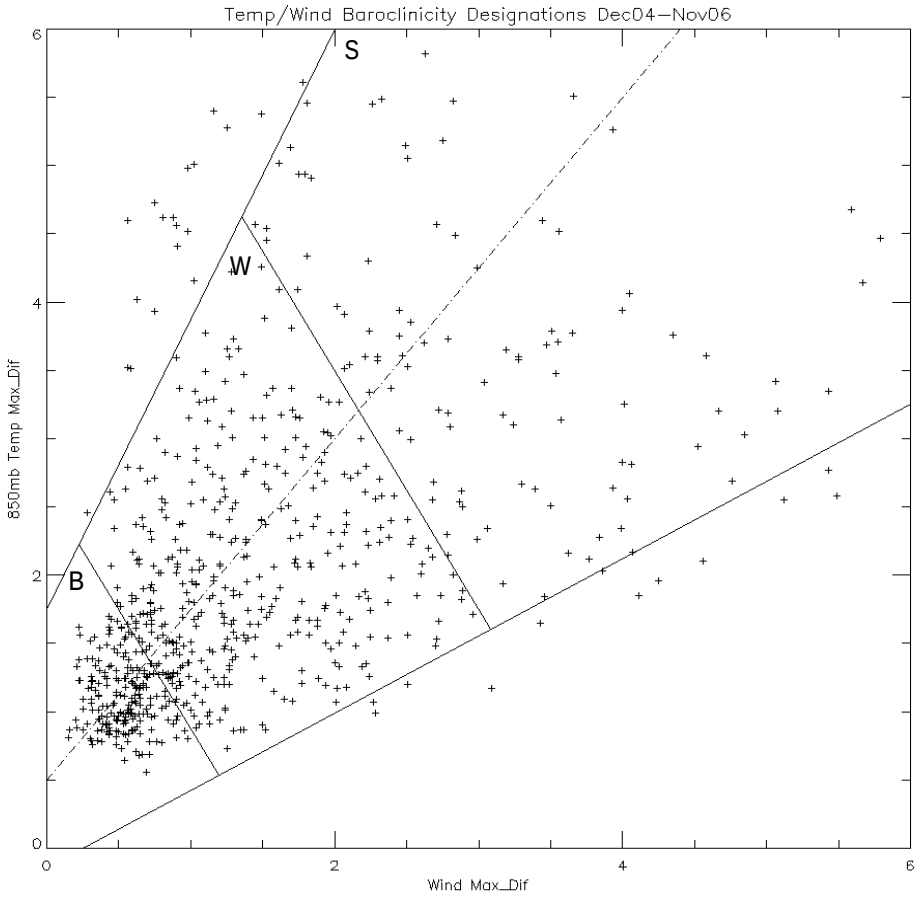

Figure 8 Baroclinicity phase-space diagram using the maximum difference in filtered 850mb temperature values over the NCEP grid and the maximum difference in filtered vertical wind shear within the 850-300mb pressure level range. The baroclinicity designations on the diagram are S-Strongly Baroclinic, W-Weakly Baroclinic and B-Barotropic.

For the 730 days of the two-year period, 214 days (29%) were identified as barotropic, 378 days (52%) weakly baroclinic, 104 days (14%) strongly baroclinic, and 34 days (5%) were outside of the designation range. A seasonal breakdown of baroclinicity designations is provided in Table 1. As expected, summer had the most barotropic days, with 79% of the days classified as barotropic, while winter had less than

1% of days classified as barotropic. Spring had the highest percentage of weakly baroclinic days (70%), with the least occurrence during summer (21%). Fall and winter also had a high frequency of weakly baroclinic (59% both). Overall, there were few strongly baroclinic days compared to barotropic and weakly baroclinic, with the highest occurrence during winter (32%). There were no strongly baroclinic days during summer, and few in spring and fall (10 and 15%, respectively). While there is some correlation between baroclinicity and seasons, the baroclinicity designations add vital synoptic information to the daily climatology.

Table 1 Seasonal breakdown of baroclinicity designations for Strongly Baroclinic (S), Weakly Baroclinic (W) and Barotropic (B). Points outside of the three baroclinicity regions were identified as n/A.

	DJF	**MAM**	**JJA**	**SON**	**Total**
B	1	26	146	40	213
W	107	128	38	107	380
S	58	18	0	28	104
n/A	14	12	0	7	33

2.2. Storm Type Climatology

A climatology of storm types based on dynamical forcing and precipitation structure was compiled for the storms identified in SE Texas during the 2-year period. Storms were identified based on a threshold accumulation observed at a ground site in College Station, Texas (30.7ºN, 96.4ºW). Further details on the surface rain measurements and storm identification can be found in Sec. 2.3. Radar imagery and

synoptic analysis charts[1] for the identified storms were used to classify the storms with an alphanumeric designation. The storm type consists of two factors, the dynamic factor and the structure factor. The dynamic factor consists of six numerical designations based on the dynamical forcings of dryline, cold front, warm front, stationary front, weak forcing and upper level disturbance. The storms are further classified with a letter designation for the structure factor, which describes the structure of the precipitation (e.g., scattered, linear, widespread) as seen using radar loops.

Analysis of synoptic conditions for the storms focused primarily on surface analysis and 700mb and 300mb charts. Possible origins of the precipitation are considered at the time of initiation of precipitation while the development of the storm was traced as it approached the ground site (i.e., College Station). The results are then used to assign the appropriate dynamic factor to the storm. The structure factor for all forcings (except the dryline and upper level disturbance cases) is determined at the time in which the storm is in its most mature stage over the ground site. The structure parameters are unique to each dynamic category. Characteristics of each storm type, with examples, will be discussed next:

---

[1] The dynamical forcing and precipitation structure for each case was determined using surface analyses, upper air charts and radar composites from the internet image archive of the Precipitation Diagnostics Group in the Mesoscale and Microscale Meteorology Division of NCAR (http://locust.mmm.ucar.edu). Example images in Figures 9-14 were obtained from this image archive.

1: Weak Forcing

Storms that develop in the absence of synoptic-scale features, such as fronts, drylines or upper level disturbances, are assigned to the weak forcing category. These storms tend to develop in SE Texas in an unstable atmosphere. There are two structure categories for the weak forcing cases (Fig. 9). Type 1a storms are small, isolated convective cells with little or no stratiform precipitation. Type 1b storms are scattered convective cells with more areal coverage and include small stratiform regions.

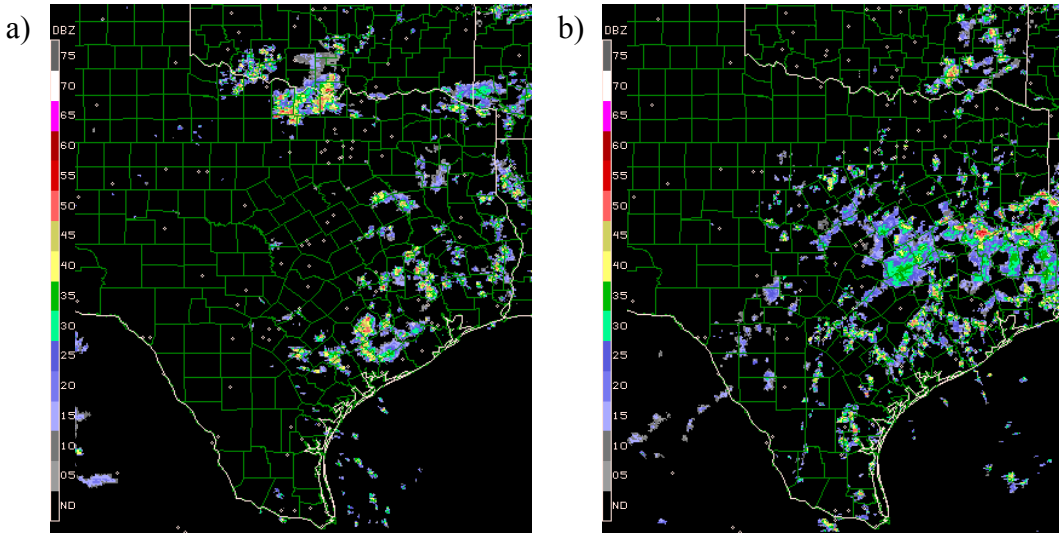

Figure 9 Example of precipitation structure for weak forcing storms a) type 1a and b) type 1b.

2: Dryline

Drylines are more common in West and Central Texas but still occur in SE Texas, particularly during the spring. In order to separate out precipitation that is forced directly by the dryline, type 2 is only assigned when there are no other synoptic scale

features present. Precipitation in dryline cases tend to be cellular but with some linear organization along the airmass boundary (Fig. 10).

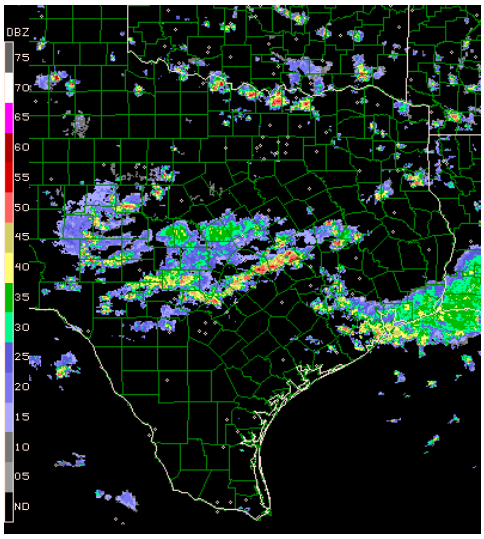

Figure 10 Example of precipitation structure for dryline storms.

3: Cold Front

The frontal boundaries of cold fronts tend to be more strongly pronounced than in other cases making classification easier. Occasionally, the precipitation lags the surface front. If by examining the upper air charts it is found that the precipitation is aligned along an upper level boundary, the storm is instead assigned to the upper level disturbance case. Three precipitation structure classes are used to divide the cold front cases (Fig. 11). Type 3a storms consist of a single, well-defined convective line with little or no stratiform precipitation. Type 3b storms have a well defined leading convective line such as in the type 3a storms, but are accompanied by a trailing

stratiform region. Type 3c storms have both convective and stratiform regions but are less organized than the 3b storms, such that the boundary between convective and stratiform regions may be less defined or the stratiform region might not be trailing the convective line.

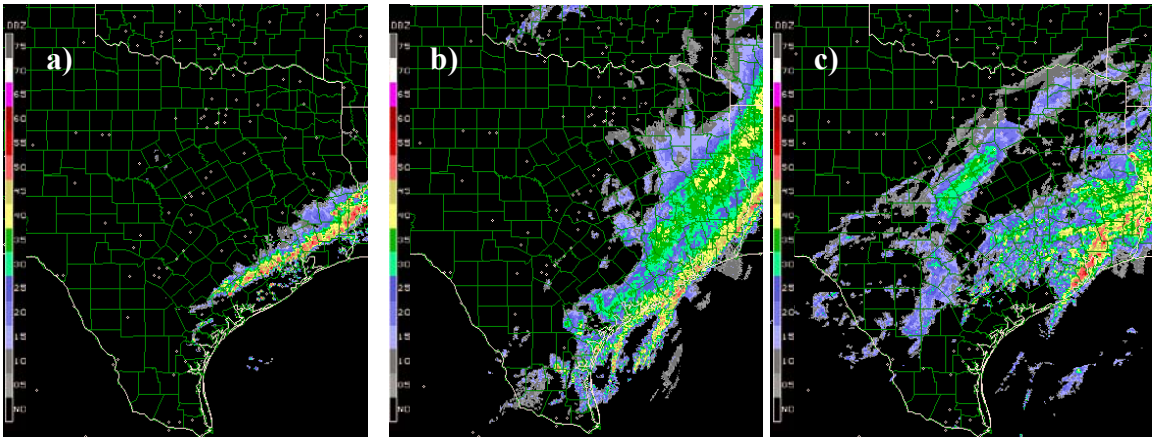

Figure 11 Example of precipitation structure for cold front storms a) type 3a b) type 3b and c) type 3c.

4: Warm Front

Storms associated with warm fronts are characterized by widespread rain ahead of the surface front as the warm air overruns the cold air (Fig. 12). Along some frontal boundaries, pockets of stronger convection can also form. Type 4a represents warm frontal storms with widespread rain and little or no convection, while type 4b is used when there is evidence of stronger convection within the widespread rain region.

a) b)

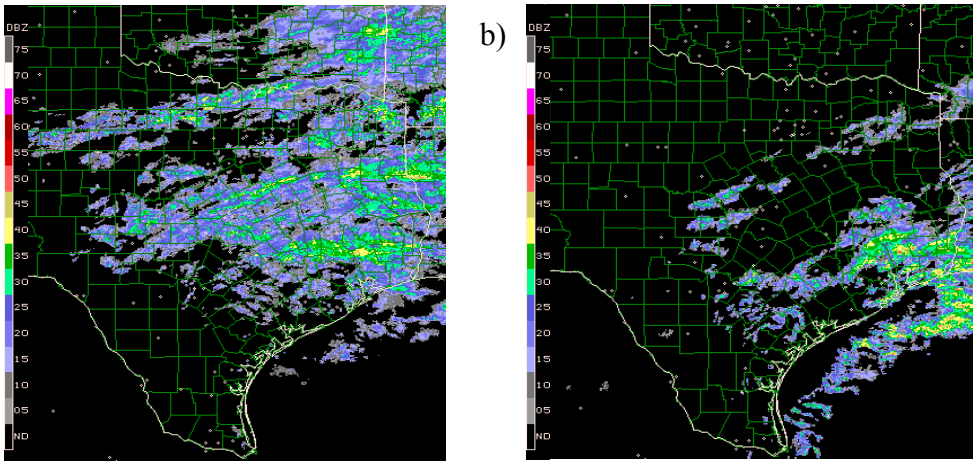

Figure 12 Example of precipitation structure for warm front storms a) type 4a and b) type 4b.

5: Stationary Front

The structure of precipitation along stationary fronts varies more than within the cold and warm front categories. This variation is due to the different warm and cold frontal characteristics that can be present during the lifetime of the stationary front. Widespread rain often accompanies stationary fronts, and there is the possibility of a concentration of convection along the frontal boundary (Fig. 13). Type 5a storms have widespread precipitation with little or no convection, whereas type 5b storms have regions of stronger convection, sometimes aligned with the surface front.

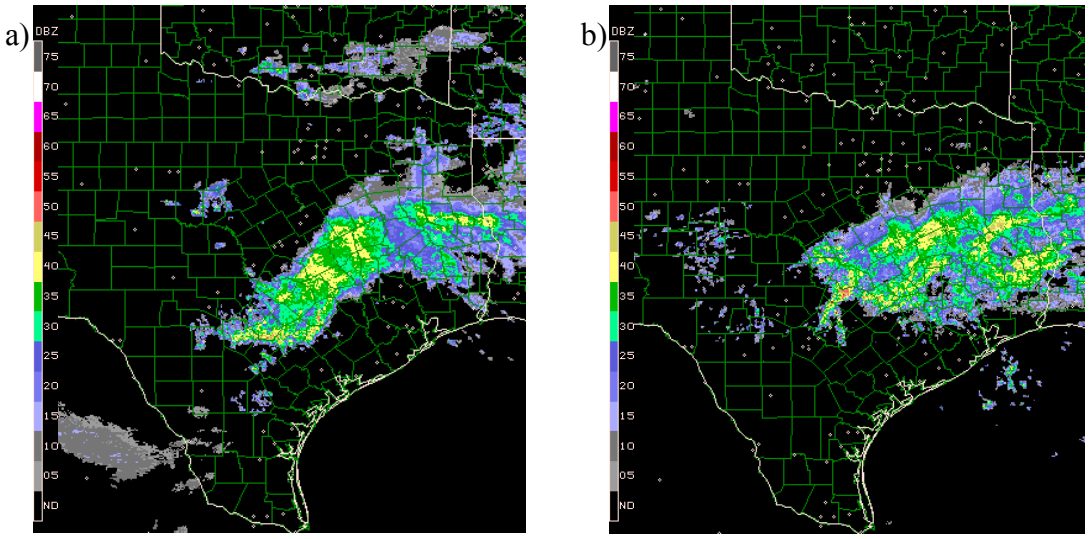

Figure 13 Example of precipitation structure for stationary front storms a) type 5a and b) type 5b.

6: Upper Level Disturbance

Upper level disturbance is a loose grouping of forcings associated with upper level features for cases where the precipitation is collocated with upper level features instead of surface features. These forcings include, but are not limited to, shortwaves, jet streaks and cutoff lows. The storms are often characterized by regions of weak, widespread precipitation (Fig. 14).

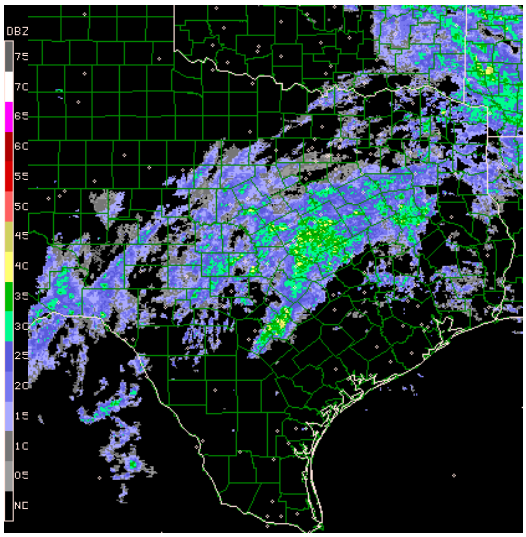

Figure 14 Example of precipitation structure for upper level disturbances.

The complete climatology of storm types consists of the 74 storms identified from the disdrometer observations (see Appendix A). A summary of the results by storm type is found in Table 2. Cold fronts are the most numerous, particularly type 3c, while warm fronts occurred less frequently than all other types. Only one storm was identified as type 4a, such that in the analysis of the climatology in Section 3.2., categories 4a and 4b will be combined into type 4. Extending the climatology through more years of data will allow for a more robust data set.

Table 2 Occurrence of radar climatology storm types for the 74 identified storms.

	1a	**1b**	**2**	**3a**	**3b**	**3c**	**4a**	**4b**	**5a**	**5b**	**6**
# storms	3	13	7	6	5	14	1	4	3	9	9

2.3. Surface Rainfall Data

Surface rainfall measurements were made by a Joss Waldvogel RD-80 (JW) disdrometer and two tipping bucket rain gauges located in College Station, Texas (30.7ºN, 96.4ºW). The instruments were installed and maintained by the Department of Atmospheric Sciences at Texas A&M University, and the site lies near the center of the NCEP reanalysis grid covering the region. Disdrometer data is available from 16 December 2004 to 30 November 2006, except from 8-29 August 2006. Both rain gauges were installed 12 August 2005 and have been in operation continuously except for a period from 11 January – 1 February 2006. The resulting data set contains 310 hours of disdrometer observations and 217 hours of rain gauge observations for analysis. The disdrometer will be the main tool for analysis, while the rain gauges are used to verify the disdrometer rain accumulations.

2.3.1. Disdrometer Measurements

The JW disdrometer converts mechanical drop impacts on a sensor with a detection area of 50 cm^2 into electronic pulses as a function of the drop diameter. The processor converts the pulses into a drop-size distribution (DSD) for use in further analysis. The disdrometer records raindrop-size distributions at 10-second intervals,

placing the data into 20 bins by drop-size ranging from 0.3mm to 5.5mm (Appendix B). The data is then re-binned into 1-minute consecutive intervals to increase sample size.

There have been many studies on error characteristics of the JW disdrometer (Sheppard 1990, McFarquhar and List 1993, Tokay and Short 1996, Tokay et al. 2003b). The primary sources of error in the measurements result from undersampling of small drops and calibration errors. There are several factors that contribute to the undersampling of small drops. First, the disdrometer is sensitive to background vibrations. When the background noise reaches the magnitude of the smallest drops sizes, the disdrometer fails to record the drops' impacts (Tokay et al. 2003b). Second, in heavy rain, the impacts of the larger drops raise the detection threshold preventing the smaller drops from being recorded at the same instant (Tokay and Short 1996). Third, windy conditions can also lead to an undersampling of small drops when their fall velocity varies from the assumed terminal fall velocity.

McFarquhar and List (1993) studied the effect of curve fits to JW disdrometer data during calibration and suggested that multiple peak DSDs are a result of instrumental errors. Recalibration of the measurements using a linear curve fit to the pre-binned data removes the erroneous peaks, resulting in a unimodal distribution. As the raw pulse data is not available for this study, the observed climatological DSD is subtracted in each individual case to reduce this calibration error such that the anomaly

from the mean distribution is analyzed. Figure 15 shows the effect of removing the climatological distribution from the individual storm DSD.

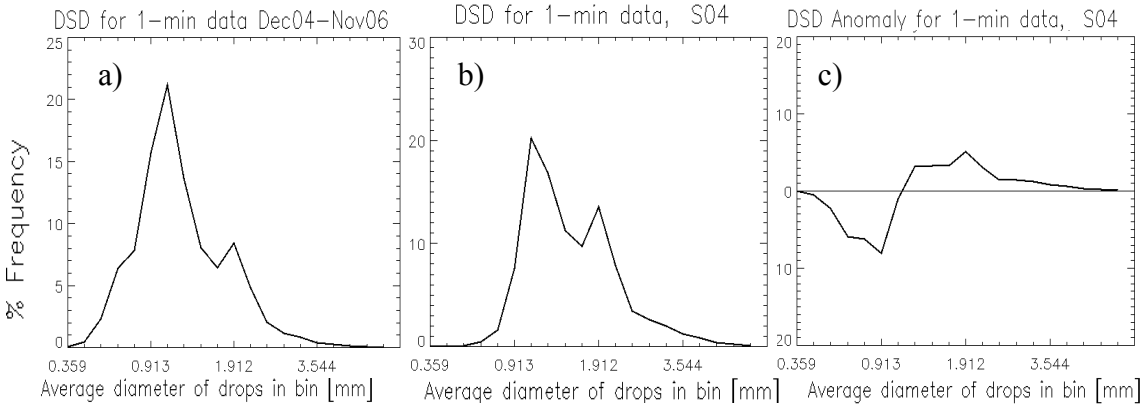

Figure 15 Effect of removing the climatological DSD from an individual storm DSD. a) Climatological Frequency DSD for December 2004-November 2006 b) individual storm DSD for storm #4 c) DSD anomaly for storm #4 calculated by subtracting b) from a).

The shapes of raindrop-size distributions change as more drops are included in the calculations, such that sampling size and variability must be considered. Joss and Waldvogel (1969) first suggested that the DSD will be more representative of the overall precipitation with a larger sample in time or space. As the spatial scale of both the rain gauges and the disdrometer are fixed, increasing the time duration of sampling is used in this study. Smith et al. (1993) conducted a numerical study of DSD characteristics based on the number of drops in a sample. A sample size of 100 drops in 1-minute will give an error of less than 1 dB for the normalized rain rate and 3 dB for the radar reflectivity factor, significantly reducing the measurement errors due to sample size (Smith et al. 1993, Steiner and Smith 2000).

2.3.2. Rain Gauge Measurements

The two tipping bucket rain gauges (identified as gauge4 and gauge6 on the data logger) tip when 0.254 mm of rainfall has accumulated in the bucket. Each tip is recorded with the data logger and labeled by a time stamp to the hundredth of a second. The tips are then combined into 1-minute intervals for comparison with the disdrometer data. The tipping bucket rain gauge is subject to wind-induced errors similar to the disdrometer, which lead to the underestimation of rainfall. Also, evaporation within the bucket volume can lead to errors in rain rate and rain accumulation calculations (Duchon and Essenberg 2001, Tokay et al. 2003). Identifying the beginning of a rain event is problematic since the time of the first raindrop is not recorded, only the time of the first tip. Therefore the time it takes to fill the bucket initially is ambiguous, whereas the disdrometer is better able to pinpoint the start and end times of the rain event (Tokay et al. 2003b).

2.3.3. Storm Identification

For the purpose of this study, disdrometer rainfall events were identified for analysis based on a variation of Steiner and Smith (2000). A minimum rain rate of 0.1 mm h^{-1} was used to identify the beginning and end of the event period. Rainfall periods with at least 4 hours of no precipitation were identified as separate events. A total

rainfall accumulation of 2.5 mm was required for an event designation and 1-minute samples with less than 100 drops were not included to decrease sample size error (see Section 2.1.1.).

Rain gauge data corresponding to rain events from the disdrometer data were identified and measurements taken between the first and last tip were included in the rain gauge event used for comparison with the disdrometer data. The first tip of each event is ignored due to the rain rate ambiguity discussed in Section 2.3.2. There were 74 storms identified during the two-year period from the disdrometer observations. A summary of rainfall parameters, baroclinicity designation and storm type for each identified storm is found in Appendix A.

2.3.4. Rain Gauge and Disdrometer Comparison

Daily rain accumulation for days with storms were analyzed for consistency between the two rain gauges (Fig. 16a). The average difference between the rain events was 7.6%, which is comparable to previous studies that found that collocated rain gauges should perform with an error of less than 10% (Habib et al. 2001b, Tokay et al. 2003b). The difference in rain accumulations between the gauges and the disdrometer is larger than between the individual gauges, with an average difference of 19%. While there is a

larger difference between the gauges and the disdrometer than between the gauges themselves, the results for both comparisons are still highly correlated.

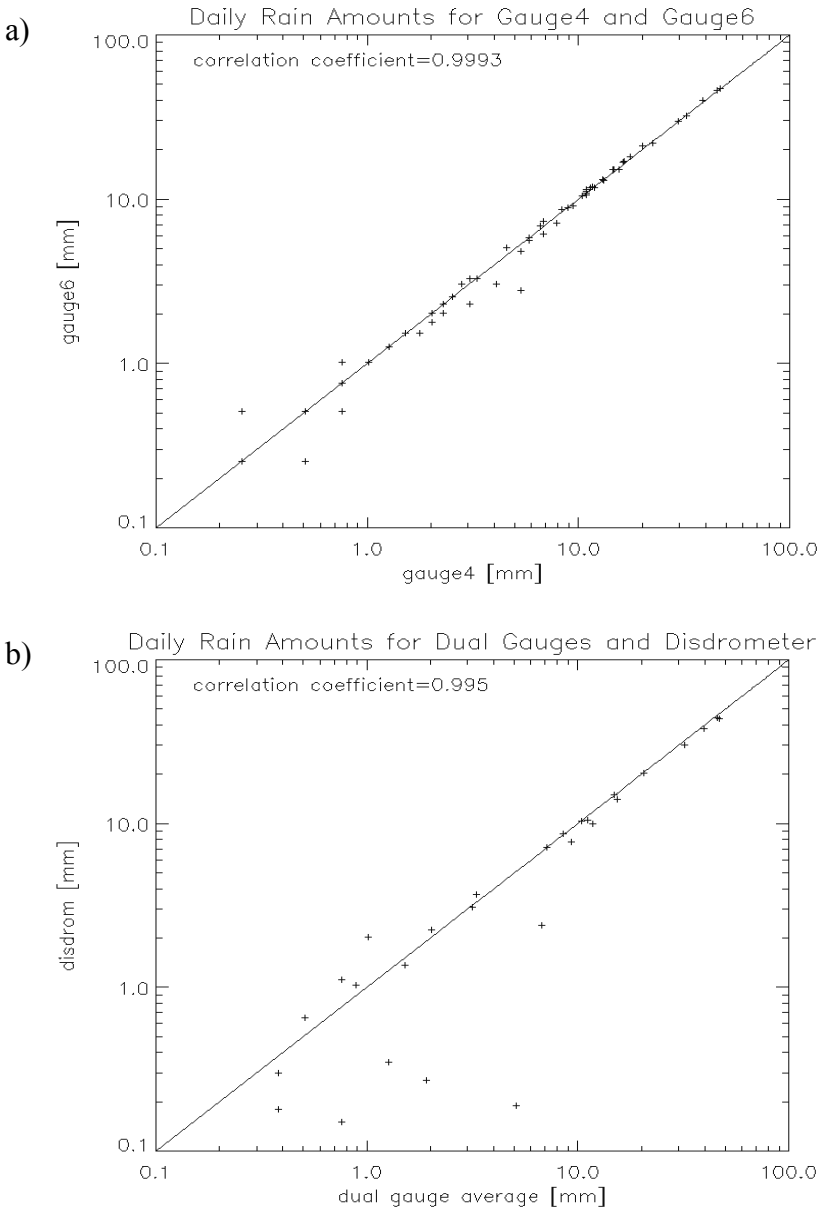

Figure 16 Comparison of surface rainfall measurements between a) gauge4 and gauge6 b) disdrometer and average gauge values.

3. RESULTS

3.1. Storms by Baroclinicity

For the two-year period of the study, 74 storms (as defined in Sec. 2.3.1.) were identified using the disdrometer observations and assigned baroclinicity designations (Fig. 17). The observations are comparable to the distribution of daily baroclinicity designations from Section 2.1.4., indicating that the storms occur in all types of environments. For the identified storms, 23 (31%) were identified as barotropic, 34 (46%) weakly baroclinic, 13 (17.5%) strongly baroclinic, and 4 (5.5%) were outside of the designation range (Table 3). Table 3 also provides a seasonal breakdown of baroclinicity designations for the identified storms. The disdrometer was only operational for a portion of SON 2006, so the values for autumn under represent the actual number of storms that occurred during that time period.

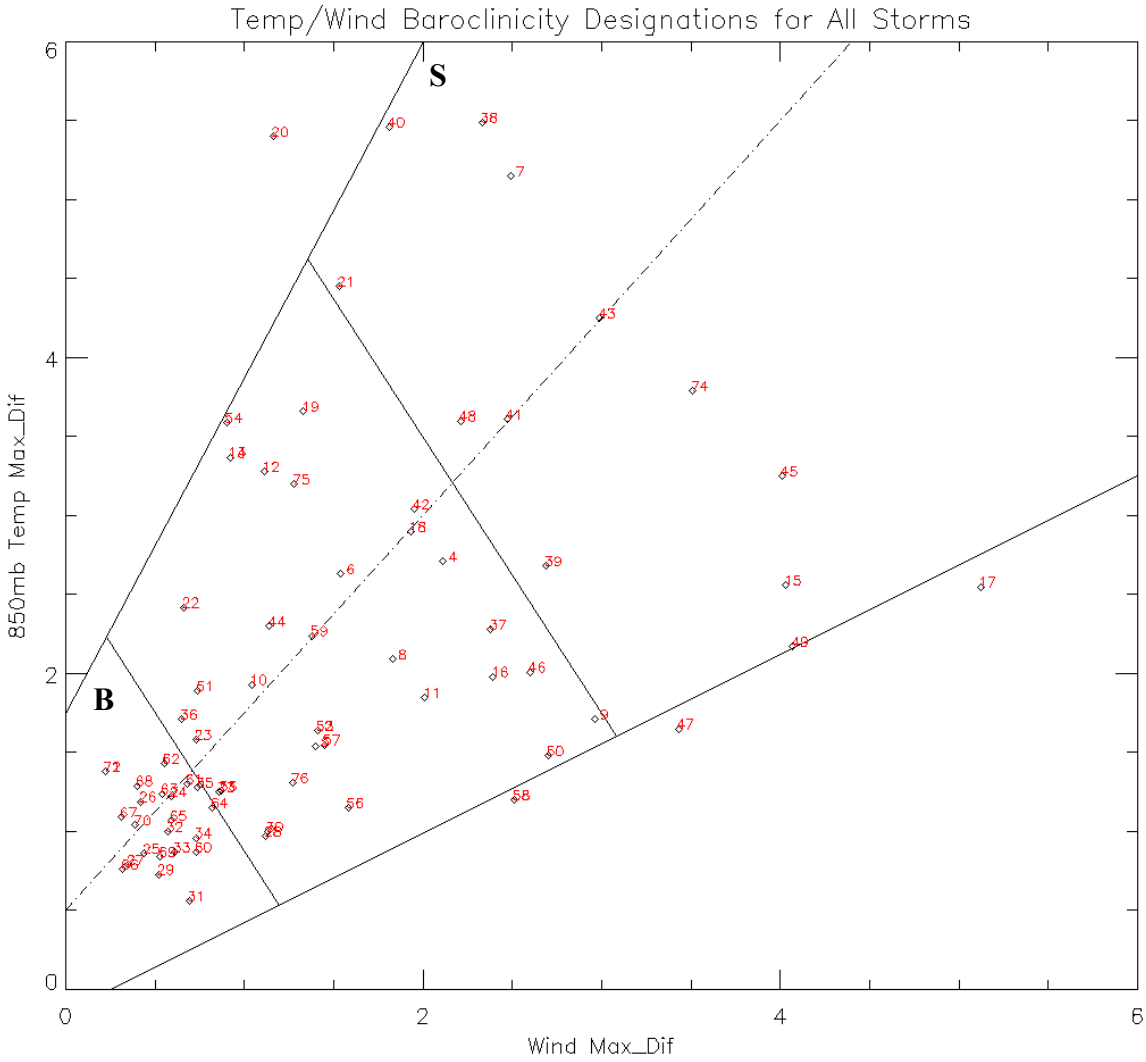

Figure 17 Phase-space diagram for all 74 storms identified from the disdrometer data. The baroclinicity designations on the diagram are S-Strongly Baroclinic, W-Weakly Baroclinic and B-Barotropic.

Eighty-seven percent of barotropic storms occurred in JJA. While there were DJF barotropic days as classified by NCEP data in the daily climatology in Section 2.1.4., there were no DJF barotropic storms observed. Seventy-nine percent of weakly baroclinic storms occurred in DJF and MAM. The weakly baroclinic storms during MAM accounted for 74% of the identified storms. More than half of the strongly

baroclinic storms were observed in DJF and 38% were observed during SON. Strongly and weakly baroclinic storms were equally represented during SON. The effect of the distribution of baroclinicity designations throughout the year will be further examined using disdrometer data in Section 3.3.

Table 3 Seasonal distribution of 74 identified storms by baroclinicity designation.

	DJF	**MAM**	**JJA**	**SON**	**Total**
B	0	1	20	2	23
W	13	14	2	5	34
S	7	1	0	5	13
n/a	1	3	0	0	4

3.2. Storm Type Climatology

3.2.1. Extreme Temperature Differences and Wind Shear

The distribution of storm types and large scale forcings as related to the corresponding daily baroclinicity designations is explored for the 74 disdrometer-identified storms (Fig. 17). However, analysis of the most extreme cases on the phase space diagram, independent of baroclinicity designation, is done first by taking the ten largest and smallest temperature difference and wind shears values. The resulting distribution of storms across the storm types is limited to those storms within the three baroclinicity regions (Table 4).

Table 4 Distribution of strongest and weakest temperature differences and wind shear by storm type for storms in B, W and S categories.

	1a	**1b**	**2**	**3a**	**3b**	**3c**	**4**	**5a**	**5b**	**6**
Strong T	0	0	0	3	2	4	1	0	0	0
Weak T	1	6	0	0	0	0	0	0	0	3
Strong U	0	0	0	0	0	4	2	0	1	3
Weak U	1	4	1	0	0	0	0	1	0	3

The strongest horizontal temperature differences were observed only in the presence of a frontal boundary, with nine of the ten being cold fronts and one warm front. This comparison supports the validity of the baroclinicity designation. The distribution within the cold front structures is fairly even. Although type 3c had more occurrences of strong temperature differences, it is important to note that more 3c storms were observed during the period of study. The four strong temperature differences in the 3c category account for only 30% of the storm type, while both type 3a and 3b had a higher percentage of strong values at 50% and 40%, respectively. Also, two of the strongest temperature differences are actually weakly baroclinic cases.

The weakest temperature differences are dominated by type 1a/b storms, which is consistent with the weak dynamical forcing in type 1 storms. The other three weak temperature difference cases were upper level disturbances, which might be disassociated from the lower level temperature field resulting in the lack of a signal in the temperature difference. The absence of frontal cases is to be expected as frontal boundaries are defined by the associated temperature difference. Only one of the weak temperature difference storms was weakly baroclinic, while the rest were barotropic.

The distribution of strongest vertical wind shear is spread over more dynamical forcing categories than the temperatures. Cold fronts make up the largest portion of these cases, followed by upper level disturbances, warm fronts, then stationary fronts. An interesting result is that all of the cold fronts in this category are type 3c. The strong wind shear influences the structure of the stratiform region relative to the convective line, which in type 3c might be the cause of the less organized structure. In addition, the strongest wind shear is not limited to strongly baroclinic cases. Three of the storms are weakly baroclinic, which are also interesting because of the corresponding weak temperature differences relative to the wind shear, emphasizing the influence of wind shear in these cases.

The storms with weak vertical wind shear are also more spread than in the weak temperature difference category. Half of the storms were type 1a/b, three were upper level disturbances, and there was one each of types 2 and 5a. All of the weak wind shear cases were barotropic. The stationary front case was the weakest front observed during the study, with both weak wind shear and temperature differences. Two of the three upper level disturbances in this category were also associated with the weakest temperature differences.

3.2.2. Frequency of Storm Types by Baroclinicity

The distribution of the identified storms by storm type and baroclinicity is contained in Table 5. The barotropic storms primarily occur under weak forcing, also drylines and upper level disturbances. Furthermore, these three dynamical forcings also

have the highest occurrence in the barotropic category. The weakly baroclinic storms are well distributed across the storm types, with the largest occurrence (29%) in type 3c and the next largest occurrence (21%) in type 5b. Frontal systems account for 79% of the weakly baroclinic storms, suggesting that the microphysics of these storms will play an important roll in the analysis of the rainfall data. In addition, 75% of stationary front cases are weakly baroclinic. Strongly baroclinic storms occur in all the frontal categories plus upper level disturbances. Cold fronts also dominate the strongly baroclinic cases, with 50% of the type 3a storms occurring in this category. Analysis of the relationship between storm type and baroclinicity using the phase space diagram will yield more insight.

Table 5 Number of storms by baroclinicity and storm type.

	1a	**1b**	**2**	**3a**	**3b**	**3c**	**4a**	**4b**	**5a**	**5b**	**6**	**Total**
B	2	11	4	0	1	0	0	0	1	0	4	23
W	1	2	2	3	3	10	0	2	2	7	2	34
S	0	0	0	3	1	3	1	1	0	1	2	12
n/a	0	0	1	0	0	1	0	1	0	1	1	5
Total	3	13	7	6	5	14	1	4	3	9	9	74

3.2.3. Phase Space Diagrams by Storm Type

The phase space diagram in Figure 17 is subdivided by storm type in order to examine the patterns in the baroclinicity designations.

1: Weak Forcing

The weakly forced storms tend to occur in barotropic environments, with three storms extending into the lower region of the weakly baroclinic region (Fig. 18). This is

primarily a result of the synoptic definition of type 1 storms, which lack features dominated by temperature differences and/or vertical wind shear, such as fronts. Type 1 storms are fairly well distributed about the center line in the lower portions of the phase space diagram, with the 1a storms scattered among the 1b storms. However, there is a difference in the average duration of the two storm types (see Appendix A): while the isolated 1a storms last only an average of 2hr, the scattered 1b storms average 8hr. The longer duration of the 1b storms may account for the greater areal extent of the stratiform regions that separate the two structure types. The smaller isolated cells that decay quickly are more likely to be assigned a type 1a classification, whereas isolated cells that survive for a longer time period are able to mature into storms that would be classified as type 1b.

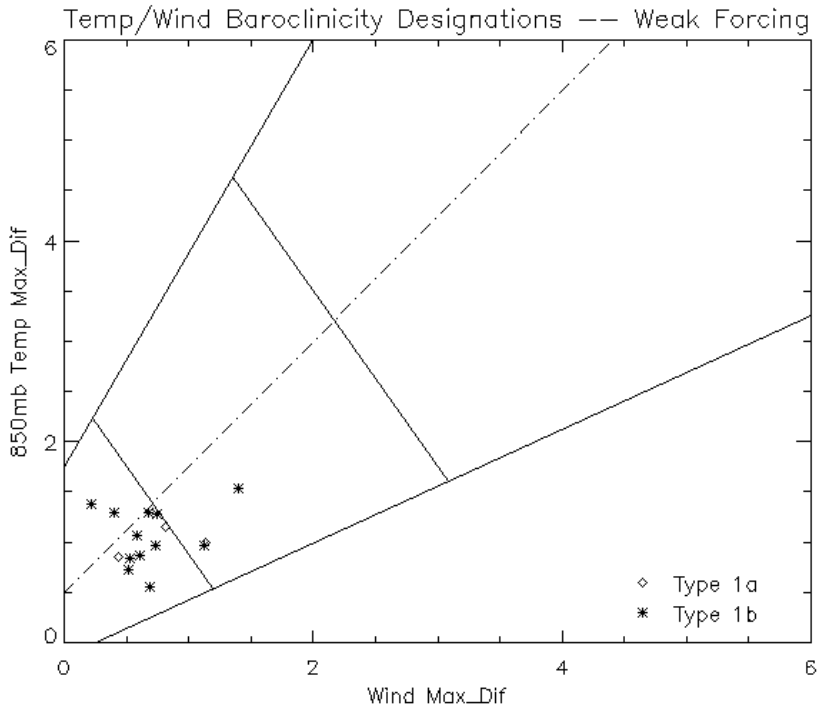

Figure 18 Phase-space diagram for weakly forced storm types.

2: Dryline

Dryline storms, like weak forcing situations, occurred primarily in barotropic environments, while the rest were weakly baroclinic (Fig. 19). The phase space diagram reveals a tendency for the type 2 storms to be located below the center line, indicating that these storms have larger vertical wind shear values relative to the temperature differences, although both are still weak. A dryline is a boundary between two air masses with different moisture contents, but not necessarily temperatures, such that the presence of a temperature difference is not required.

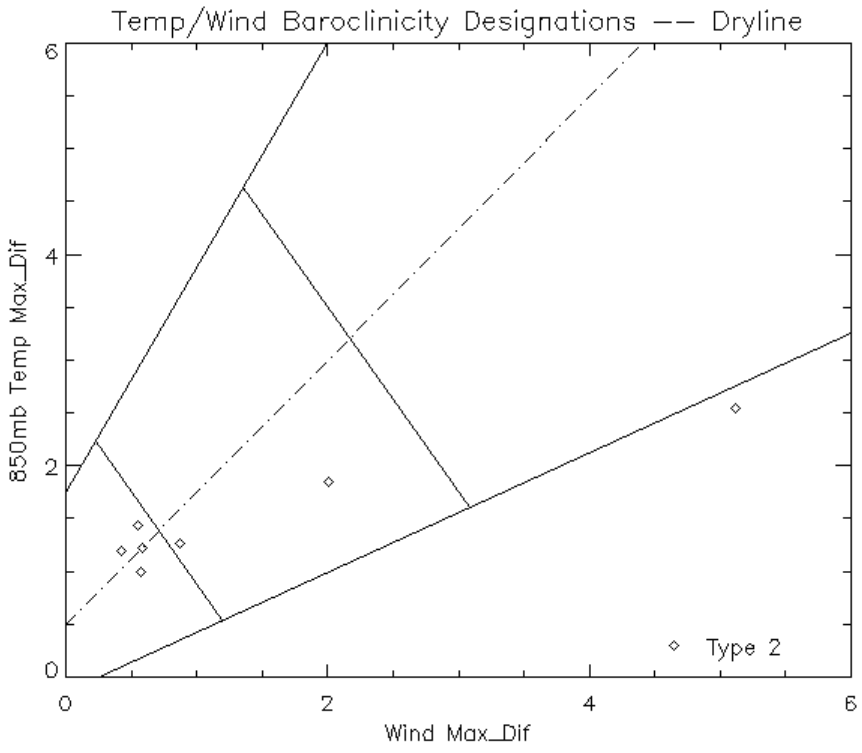

Figure 19 Phase-space diagram for dryline storm types.

3: Cold Front

The cold frontal storms were well observed with 25 systems over the 3 structure types during the observation period (Fig. 20). Type 3c storms were the most numerous, owing to the more extensive structure definition. The cold fronts with only a convective line (type 3a) show a tendency to have stronger temperature differences relative to the vertical wind shear. The lack a strong wind shear anomaly could be keeping the focus of the convection directly above the surface front, hindering the formation of a stratiform region. The 3b leading line, trailing stratiform storms have a somewhat similar distribution to 3a storms. It is possible that the presence of a stratiform region in the 3b storms compared to the 3a storms is due to other factors, such as available moisture at midlevels, which would be an interesting topic for further study.

The many 3c storms tend to cluster around the center line, suggesting that the importance of the temperature difference versus the wind shear is more equal although variations in the relative importance occur from storm to storm. The tendency toward stronger wind shear compared to the 3a/b cases could explain the less organized structure that is characteristic of the 3c storms. In these storms, the stratiform precipitation does not trail directly behind the convective line.

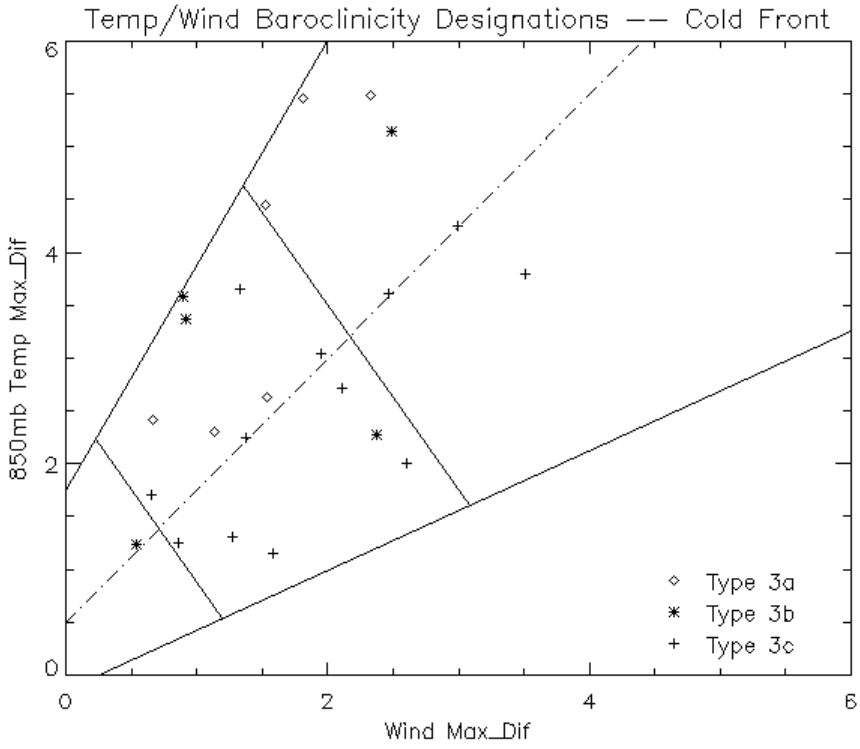

Figure 20 Phase-space diagram for cold front storm types.

4: Warm Front

Warm front storms occurred the least, with only 5 observed during the study period. Since there was only one storm classified as 4a, for the purposes of this analysis, both structure types will be combined into a general type 4 category. However, the two will remain separate for a future, longer term climatology in case variations between the two storm types might be revealed with more observations. The warm frontal storms tend to be located below the center line, indicating stronger wind shear relative to the temperature difference, and the warm fronts generally have weaker temperature differences than cold fronts (Fig. 21, Fig. 20).

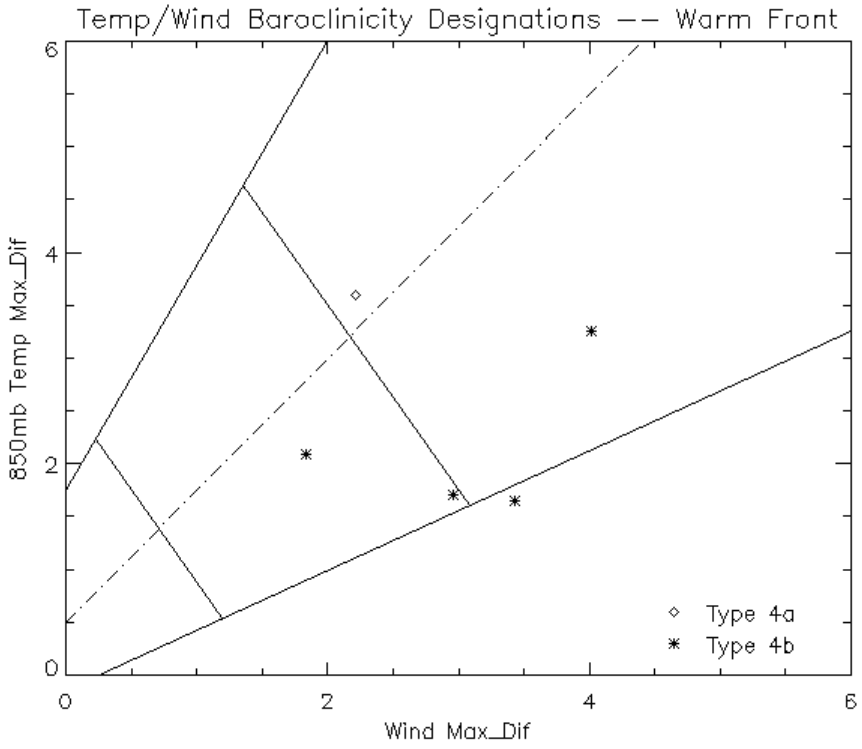

Figure 21 Phase-space diagram for warm front storm types.

5: Stationary Front

The stationary front storms are predominantly weakly baroclinic (Fig. 22). Type 5a storms, which exhibit widespread precipitation, tend to have weaker temperature differences and wind shear than the 5b cases, which include pockets of stronger convection. The stronger forcing in the 5b cases could allow for the development of stronger convection within the widespread precipitation. The majority of the 5b storms are also located below the center line, suggesting that the stronger wind shear in particular might be responsible for enhancing the convection.

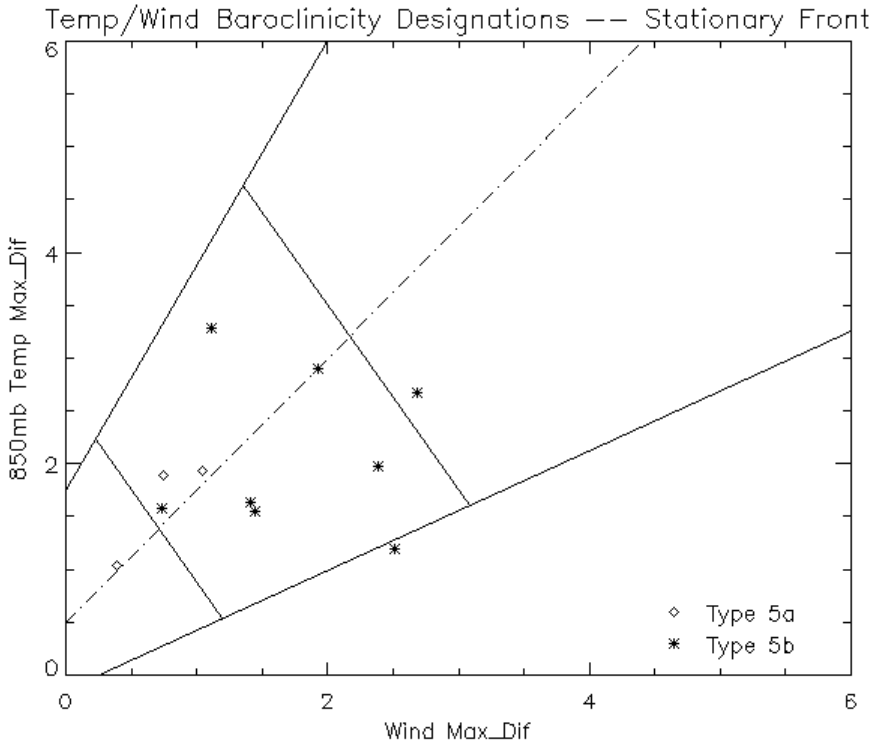

Figure 22 Phase-space diagram for stationary front storm types.

6: Upper Level Disturbances

The upper level disturbance cases show a wide spread in the phase space diagram (Fig. 23). While half the storms are barotropic, the weakly and strongly baroclinic regions each contain a remaining quarter of the storms. This bifurcation is most likely a reflection of the varied storm types that could be contained within the category. Upper level disturbances include forcings at different pressure levels. Subdividing the category by pressure level, for instance by 250mb and 700mb, could reveal clustering on the diagram. There were 3 upper level disturbances in the strongest wind shear category and 3 different storms in the weakest wind shear category (Sec. 3.2.1.). The cases of

strongest wind shear could be associated with the subtropical jet stream whereas the weak wind shear cases are more likely associated with midlevel features, such as shortwaves, which are less often accompanied by strong wind shear.

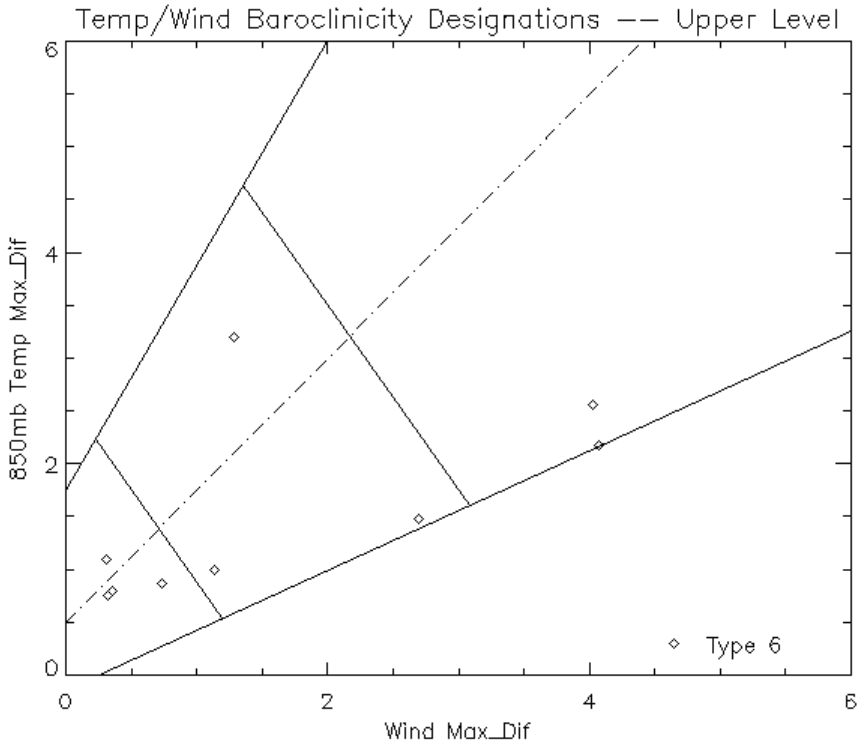

Figure 23 Phase-space diagram for upper level disturbance storm types.

3.3. Surface Rainfall Observations

3.3.1. Climatological Drop-Size Distribution (DSD)

The climatological DSD for all 74 storms identified from the disdrometer data is found in Figure 24. This normalized distribution is the basis for further DSD comparisons by season, baroclinicity and storm type. The DSDs for each of these categories will be subtracted from the total distribution, leaving only the DSD

anomalies. Besides decreasing the influence of systematic instrumental errors (Sec 2.3.1.), removing the mean distribution allows for an easier analysis of the DSD variations between categories. The drop-size modes (very small, small, medium and large) that will be used throughout the discussions are identified on the figure. Also note that the tick marks on the x-axis of Figure 24 (and subsequent DSD figures) represent the preset JW disdrometer bins (see Appendix B) and are not strictly linear.

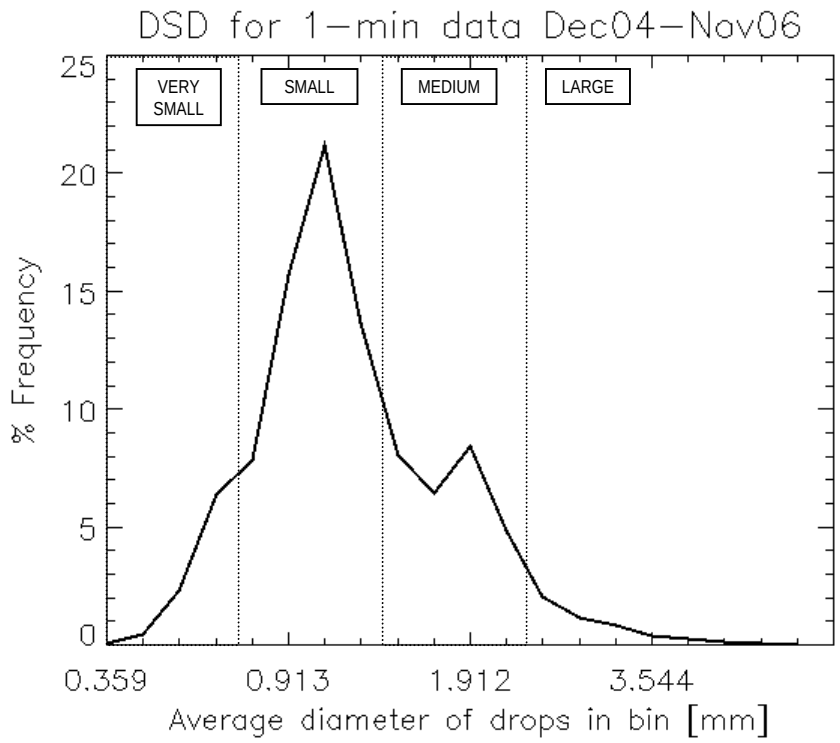

Figure 24 Climatological DSD for the two-year study period. Drop-size modes of very small, small, moderate and large are identified on the figure.

Understanding the variation of drop-size distributions is important, but incomplete without an accompanying discussion of the microphysical processes

responsible for the distribution. Steiner and Smith (1998) related the droplet formation mechanisms to the resulting droplet size recorded at the surface. The very smallest drops are the result of the weakest convection. The small drop mode is characteristic of weak to moderate convection as weak updrafts in the convective core lead to the formation of small ice crystals that melt to create small rain drops. The medium drop mode is primarily a feature of stratiform regions in which aggregates of ice crystals melt below the bright band region of mature mesoscale systems, yielding an abundance of medium drops. The large drop mode is found only in the strongest convection where large graupel melts to form the largest drops.

3.3.2. Seasonal DSD

The drop-size distributions for all storms collected over the two-year period were broken down by season. The normalized frequency distributions for each season were then subtracted from the total normalized distribution from Sec. 3.3.1. (Fig. 25). The DSD anomalies vary widely between seasons and even between the same season in different years.

The DJF DSD anomalies show the most similarities between years compared to the other seasons. Both winter DSDs have more smaller drops and a deficiency in medium to large drops. The SON 2006 DSD is also similar to these winter distributions, but with fewer very small, medium and large drops, and an even greater amount of small drops compared to the average DSD. These three distributions can be summarized by an

excess of small drops and a lack of medium to large drops, representing a propensity for storms with widespread, weak convection.

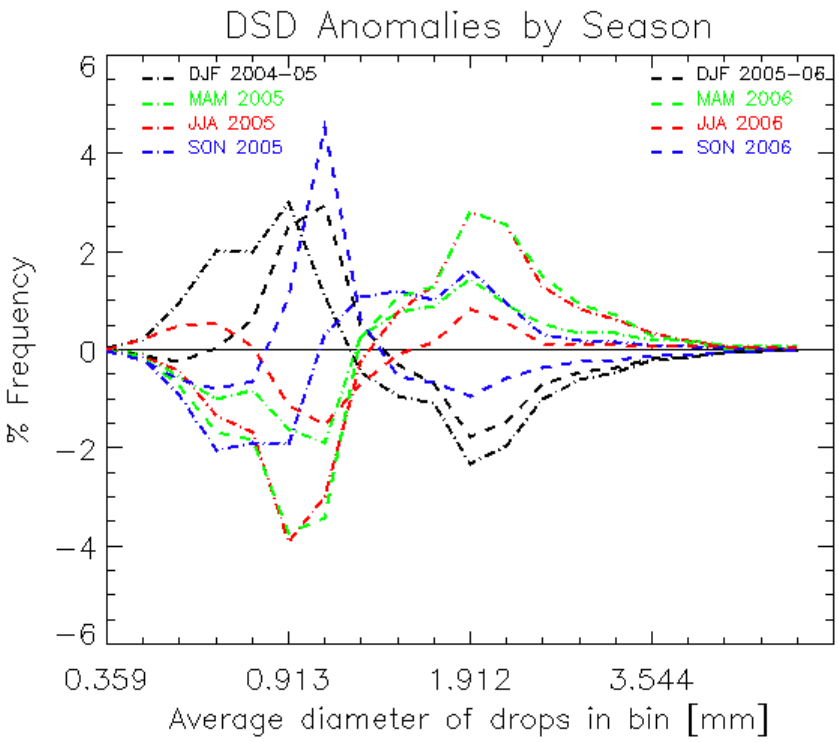

Figure 25 DSDs by season for December 2004 – November 2006.

The MAM 2006 and JJA 2005 distributions are nearly identical, and can be described as reflections of the winter distributions across the zero line. There are fewer small drops observed in the distributions and more medium to large drops. The larger drops observed indicate that storms with strong convection accompanied by stratiform precipitation play a considerable role during these seasons.

The MAM 2005, SON 2005 and JJA 2006 anomalous distributions are less pronounced than those discussed previously. Of these three distributions, the SON 2005

DSD has the fewest very small drops, but has the most medium to large drops; the JJA 2006 distribution has the most small drops and the fewest medium drops; MAM 2005 is more similar to the JJA 2006 distribution in the very small region, but is closer to SON 2005 at larger drop-sizes. Even though these distributions are more moderate than the MAM 2006 and JJA 2005 distributions, they are still characterized by relatively fewer small drops and more medium to large drops, suggesting that storms with only weak convection and storms with stronger convection and stratiform precipitation occurred.

While it is possible to group the DSDs by the distributions in Figure 25, the clustering is not consistent within seasons. The segregation of the DSDs by season is therefore insufficient for describing storm microphysics, and a different basis for analysis is necessary.

3.3.3. Drop-Size Distributions by Baroclinicity Designations

Separating the DSDs by baroclinicity yields three distinct distributions (Fig. 26). The barotropic DSD is dominated by the medium and large drop modes, with a deficiency in very small and small drops. On the other hand, the strongly baroclinic DSD is dominated by the very small and small drop modes, but deficient in the medium and large drop modes. The weakly baroclinic DSD is more moderate than the barotropic and strongly baroclinic DSDS, but is weighted towards the small drop mode, similar to the strongly baroclinic distribution.

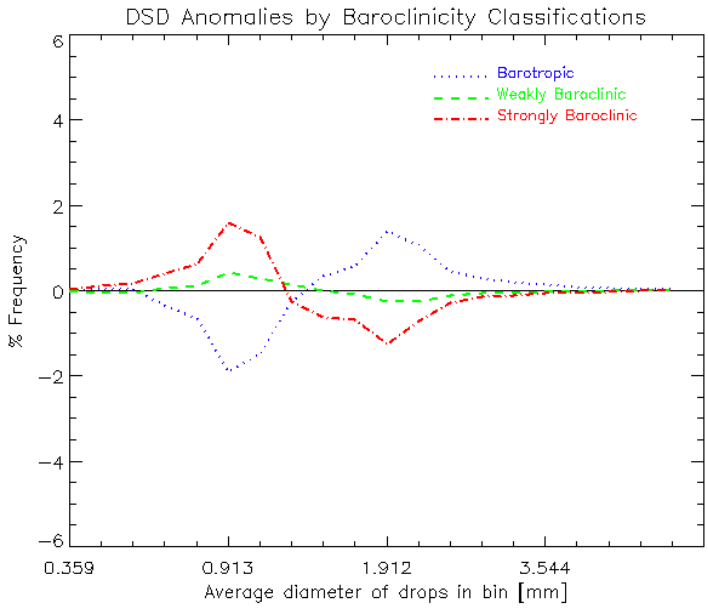

Figure 26 Climatological DSDs by baroclinicity for barotropic, weakly baroclinic and strongly baroclinic regimes.

Based on the DSDs, we can hypothesize about the associated storm microphysical processes. Barotropic storms would be expected to have strong convection with accompanying stratiform regions. The lack of small drops could be the result of evaporation due to warmer surface air temperatures that frequently accompany barotropic environments.

Strongly baroclinic storms account for a much higher percentage of the small drops, indicating the importance of weak to moderate convection, although stratiform precipitation is crucial to frontal storm types within the strongly baroclinic regime (see Sec. 3.3.4.). The weak convection could be a reflection of the lower vertical extent of many strongly baroclinic storms, which would inhibit the development of extensive stratiform regions.

The more moderate weakly baroclinic DSD is a combination of smoothing due to a larger number of storms in this category, and the conflicting nature of the storm type DSDs (Sec. 3.3.4.). Widespread weak convection would contribute to the weakly baroclinic small drop modes, whereas the stratiform and deep convective precipitation from squall lines and MCSs would contribute to the medium drop mode. While variability still exists within the regimes, the baroclinicity designations provide a foundation for future analysis.

3.3.4. Storm Type DSDs

Subdividing the total DSD by storm type yields more storm-specific information than the baroclinicity distributions alone (Fig. 27). The small drop mode is dominated by the warm frontal storms (type 4), with additional contribution from the upper level disturbances (type 6), which would be the result of weak, widespread precipitation. The medium to large drop modes are dominated by cold (type 3) and stationary (type 5) front DSDs, which are nearly identical. The DSDs that are weighted towards larger drops are typical of strong convection with accompanying stratiform precipitation. The weakly forced (type1) normalized DSD anomaly is near zero, indicating the drop-size modes have a relatively equal weight within the distribution. The dryline (type 2) distribution has more smaller drops, but the peak is lower than in the upper level disturbance and warm front DSDs and shifted towards slightly larger drops. Further subdividing storm types 1, 3 and 5 by structure will help to explain how the individual storm DSDs

influence the climatological DSDs (Fig. 28). Recall that storm types 2, 4 and 6 are not subdivided by precipitation structures.

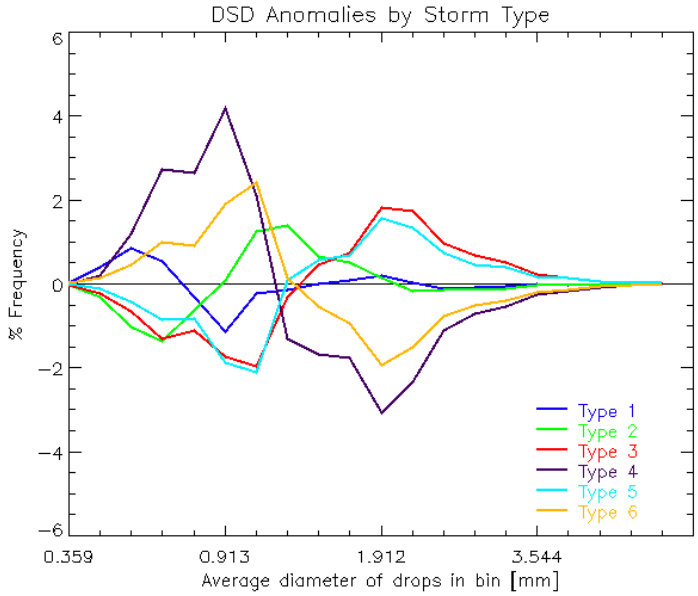

Figure 27 Climatological storm type DSDs.

The DSD anomalies for storm types 1a/b (Fig. 28a) are distinctly different (i.e., type 1a shows a large positive anomaly at larger drop-sizes and a large negative anomaly at smaller drop-sizes while the type 1b distribution is fairly flat) but do not contribute equally to the total type 1 DSD. There were only three type 1a storms, while there were 13 type 1b storms observed. An important influence on the DSDs for the type 1 storms is the horizontal extent of the precipitation. The disdrometer is a point observation, only capturing precipitation that passes directly over the small sensor. The type 1 storms tend

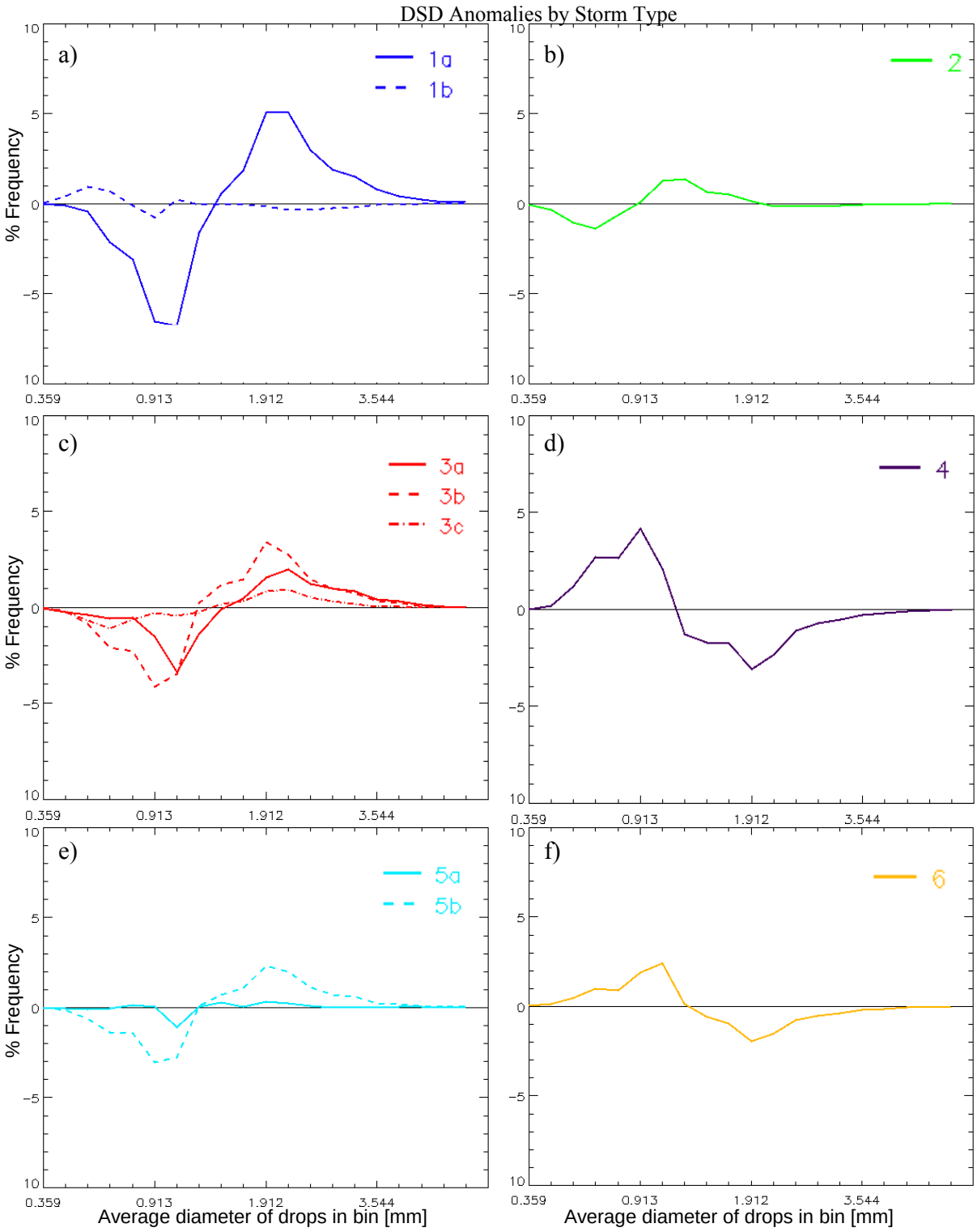

Figure 28 Climatological storm type DSD anomalies for a) weak forcing b) dryline c) cold front d) warm front e) stationary front f) upper level disturbance.

to be isolated cells, such that the portion of the storm that is measured may not be representative of the whole. Particularly in the type 1b cases where both convective and stratiform precipitation exists, the disdrometer might only measure either the convection or the stratiform, resulting in DSDs that would cancel out in the total distribution.

The general DSD anomalies are consistent across the structure categories for type 3 storms, with a predisposition towards medium to large drops (Fig. 28c). The type 3b DSD has the highest bias towards medium to large drops, which indicates strong convection with accompanying stratiform region, consistent with the structure definition of leading line-trailing stratiform (LLTS) storms. It is therefore reasonable to conclude that the type 3b approximates the expected LLTS drop-size distribution. The type 3a DSD is also weighted towards larger drops, but has fewer medium drops than the type 3b DSD, due to the lack of a stratiform region in type 3a storms. The type 3c distribution is more equally weighted between the small and medium drop modes, although still biased towards the larger drops, suggesting that there is more weak convection along with the stratiform and strong convective precipitation.

The type 5a DSD anomaly is close to zero (Fig. 28e), which indicates that the 5a storm type can be approximated by the total climatological distribution . The type 5b DSD is weighted towards medium to large drops, and is similar to the type 3b DSD, which might suggest that the precipitation resembles LLTS storms.

3.3.5. Combined Baroclinicity and Storm Type DSD Analysis

The drop-size distributions by baroclinicity regime from Figure 26 are subdivided by storm type (Fig. 29). For the barotropic regime, the storm type DSDs work in unison to create the pronounced large medium to large drop modes, particularly in types 2, 3 and 5. The distinct storm type DSDs under the weakly baroclinic regime work against each other such that the resulting total weakly baroclinic DSD anomaly is near zero. The enhanced small drop mode in storm types 2, 4 and 6 are typical of widespread, weak convection whereas the enhanced large drop mode in storm types 3 and 5 are typical of strong convection with robust stratiform regions. Only four storm types are represented in the strongly baroclinic DSD, three of which (storm types 4, 5 and 6) combine to form the dominant small drop mode. The type 3 DSD is constant across all three baroclinicity regimes, suggesting that the storm dynamics are responsible for the shape of the DSD and the environmental baroclinicity modifies the strength of the peak.

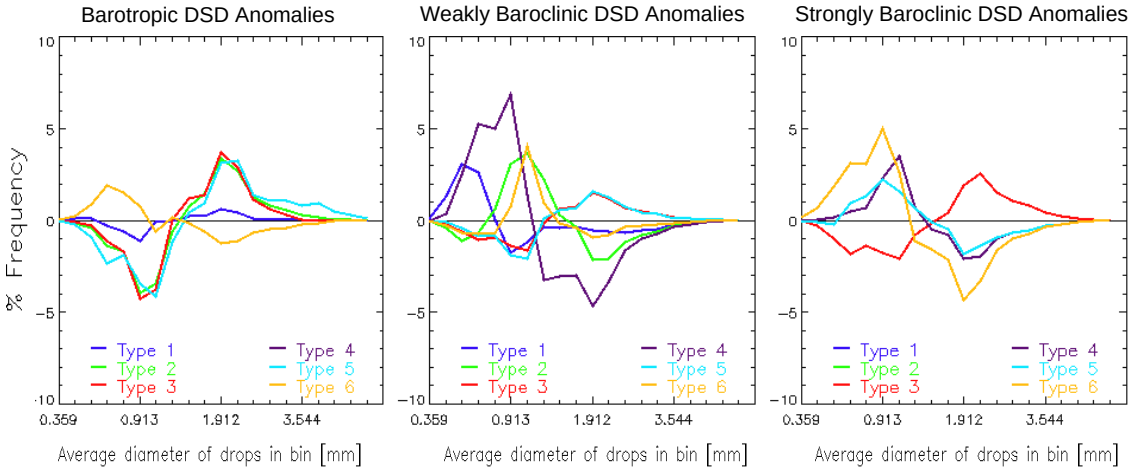

Figure 29 Baroclinicity DSDs by storm type for a) barotropic b) weakly baroclinic and c) strongly baroclinic regimes.

The drop-size distributions by storm type from Section 3.3.4. are also analyzed for variations across baroclinicity designations:

1: Weak Forcing

Separating the weakly baroclinic and barotropic DSDs of the weakly forced type 1 storms yields distributions that vary most in the very small drop modes (Fig. 30a). Subdividing by structure reveals that the type 1a storms do not vary greatly between baroclinicity regimes (Fig. 30b). The type 1b storms have more weight than the 1a storms on the baroclinicity DSDs in Figure 30a due to the higher number of storms in the climatology, particularly in the barotropic regime. In order to uncover why the barotropic 1b DSD anomaly is close to zero, the individual storm DSDs were examined (Fig. 30c). Two patterns in the distributions were identified; half of the storm DSDs were weighted towards small drops and the other half were weighted towards medium drops. This separation is most likely the result of the sampling errors discussed in Section 3.3.4. The smaller drop DSDs would be sampled from shallow convection, while the medium drop DSDs would be from the stratiform region associated with deep convection. Future radar analysis would provide data in the vertical allowing for comparisons across the entire radar volume.

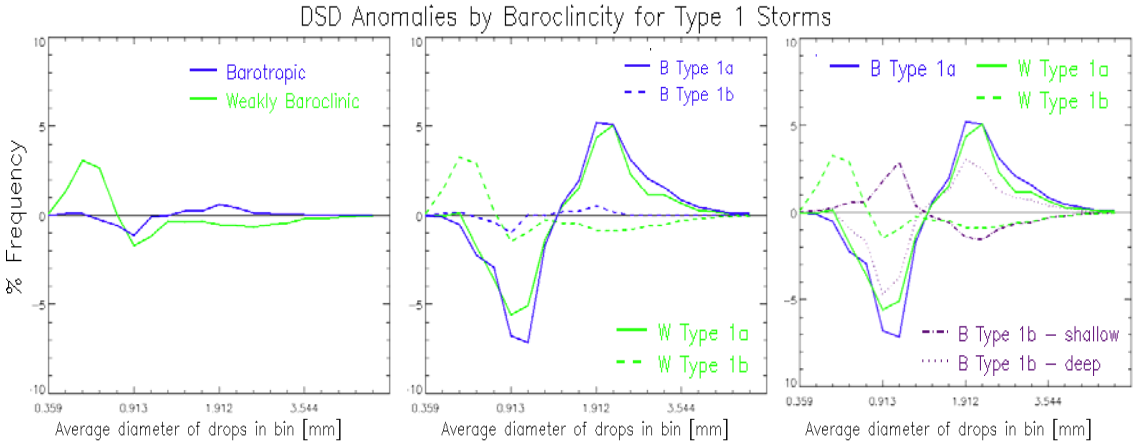

Figure 30 Type 1 DSDs by a) baroclinicity b) baroclinicity and structure c) same as b) but separating the shallow convective and stratiform precipitation.

2: Dryline

The barotropic and weakly baroclinic type 2 distributions are mirror images of each other (Fig. 31). The barotropic type 2 DSD is consistent with the climatological barotropic distribution, with a predisposition towards strong convection and stratiform precipitation. The weakly baroclinic type 2 DSD is instead shifted towards smaller drops, which suggests that the convection associated with the dryline is weaker than under the barotropic regime.

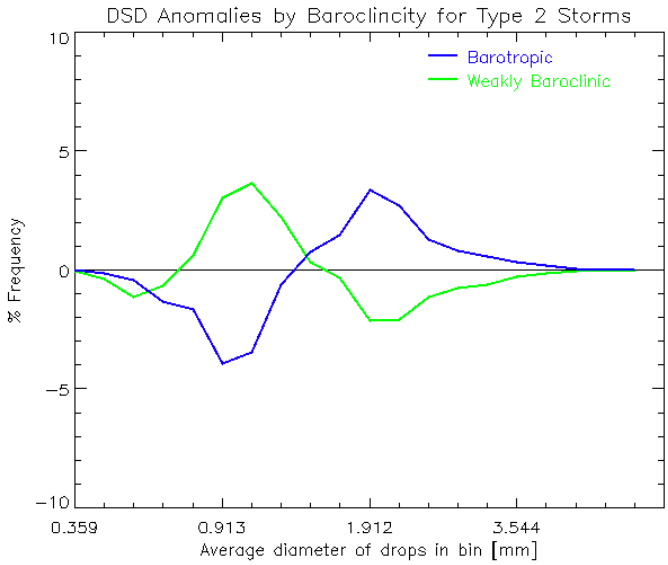

Figure 31 Type 2 DSDs by baroclinicity.

3: Cold Front

Type 3 DSDs are fairly uniform across the baroclinicity categories, exhibiting a high frequency of medium to large drops (Fig. 32a). The strongly baroclinic type 3 distribution is shifted more towards larger drops than the weakly baroclinic type 3 DSD, suggesting that the strongest convection found in cold frontal storms is found in the strongly baroclinic cases. The cold frontal weakly and strongly baroclinic DSDs were separated by structure (Fig. 32a,b). The type 3b distributions show the most similarities between baroclinicity. The weakly baroclinic type 3a distribution is weighted towards small drops whereas the strongly baroclinic is weighted heavily towards large drops, suggesting that the convection that defines the type 3a storms is stronger under the

strongly baroclinic regime than the weakly baroclinic, perhaps due to enhanced frontal lifting in the strongly baroclinic cases.

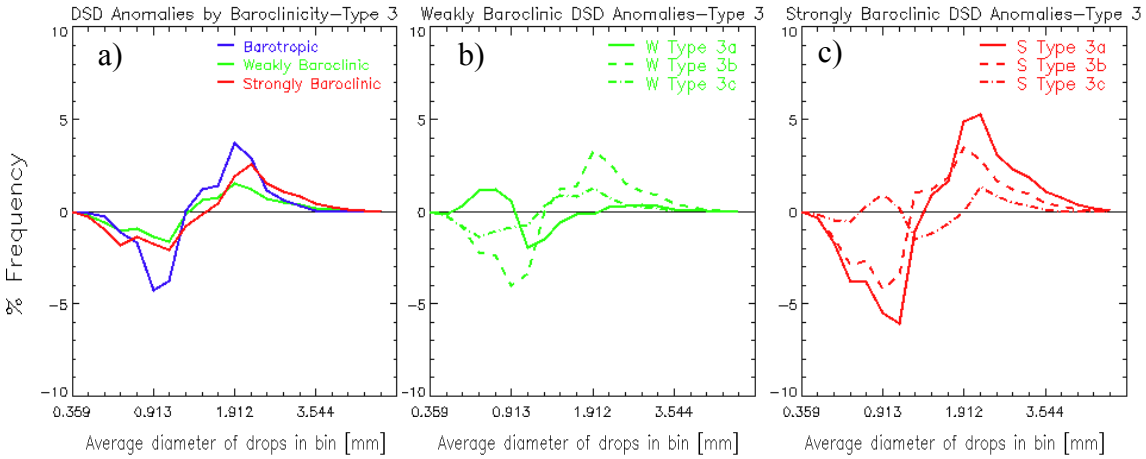

Figure 32 Type 3 DSDs a) by baroclinicity b) for weakly baroclinic storms by structure c) strongly baroclinic storms by structure.

4: Warm Front

Both the weakly and strongly baroclinic warm frontal distributions are dominated by smaller drops, although the peak drop-sizes vary (Fig. 33). The weakly baroclinic DSD is heavily weighted towards the very small drops, indicating weak widespread precipitation. The strongly baroclinic DSD is shifted towards the small drop mode and peaks at a more moderate frequency, indicating that there is some deeper convection associated with the weaker widespread precipitation.

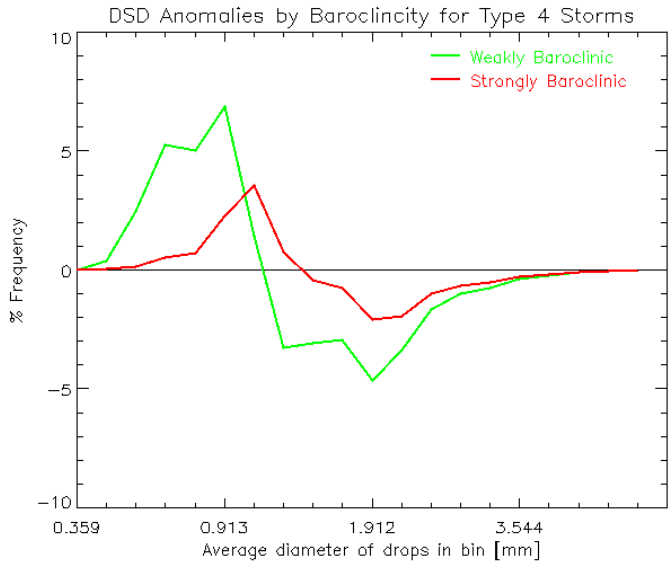

Figure 33 Type 4 DSDs by baroclinicity.

5: Stationary Front

Subdividing the stationary front DSDs by baroclinicity does not yield definitive results, as there is only one each of the strongly baroclinic and barotropic storms (Fig. 34a). However, the resulting DSDs are consistent with what we would expect based on the climatological baroclinicity distributions in Figure 26. The strongly baroclinic and barotropic type 5 DSDs closely resemble their respective climatological distributions. The weakly baroclinic type 5 DSD is more moderate than either the barotropic or strongly baroclinic DSDs, but weighted towards larger drops than in the climatological weakly baroclinic distribution. The type 5 weakly baroclinic storms separated by structure closely resemble the total type 5a/b DSDs in Figure 28e, which is due to the frequency of type 5 storms by baroclinicity (Fig. 34b). The weakly baroclinic type 5b

storms are weighted towards larger drops, a reflection of the stronger convection present within the storm that is used to identify the structure.

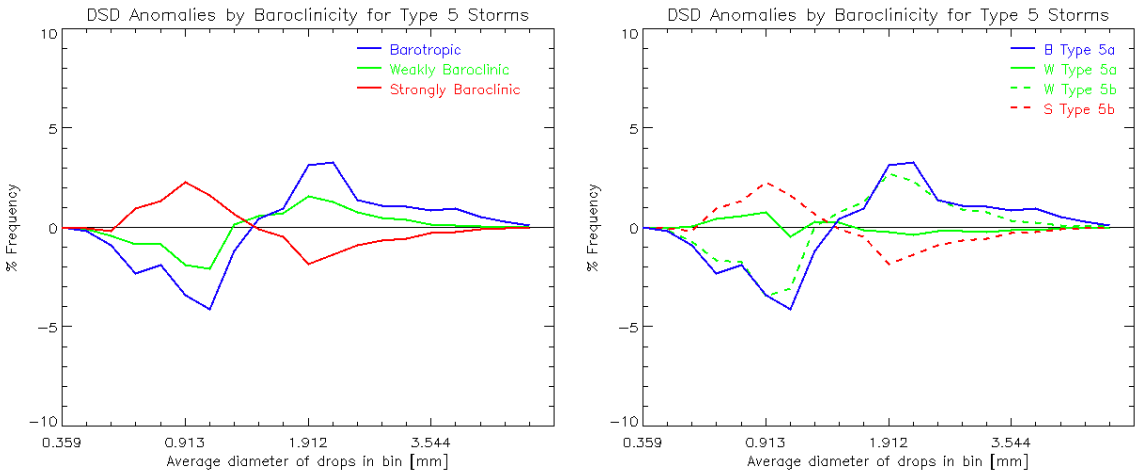

Figure 34 Type 5 DSDs by a) baroclinicity and b) structure for the weakly baroclinic storms.

6: Upper Level Disturbance

The type 6 baroclinicity DSDs all show a tendency towards small drops, which act in unison to create the climatological type 6 distribution (Fig. 35). The barotropic DSD peaks in the very small drop mode, whereas the weakly and strongly baroclinic DSDs peak in the small drop mode. The strongly baroclinic distribution has the highest frequency of small drops, although the peak in the weakly baroclinic distribution is concentrated within a much smaller drop-size range, indicating less variation in the precipitation within the storms.

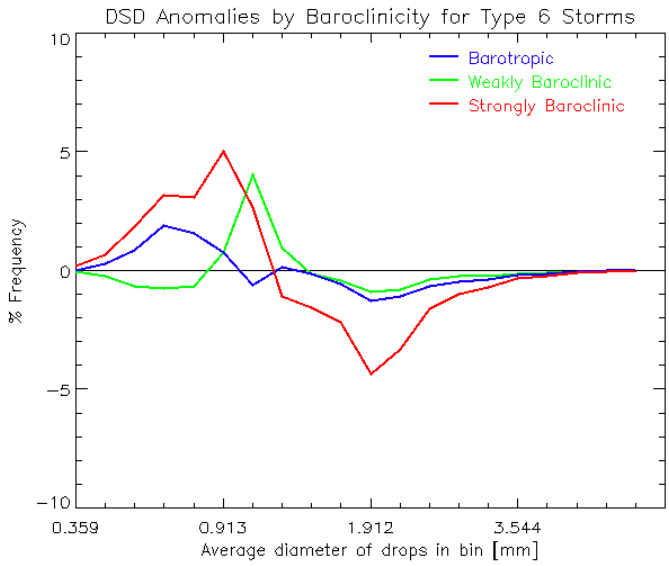

Figure 35 Type 6 DSDs by baroclinicity.

3.3.6. Climatological DSDs by Rain Rate

The drop-size distributions were divided into four rain rate ranges (Fig. 36): R1 less than 1mm h^{-1}, R2 1-5mm h^{-1}, R3 5-25mm h^{-1}, and R4 greater than 25mm h^{-1}. The rain rates in category R1 are typical of weak rain; R2 rain rates are typical of weak convection or moderate stratiform rain; R3 represents moderate convection or strong stratiform rain; R4 is found only in strong convection. As would be expected, the DSD values shift from positive anomalies in the smaller drop modes at weaker rain rates to positive values in the larger drop modes at stronger rain rates.

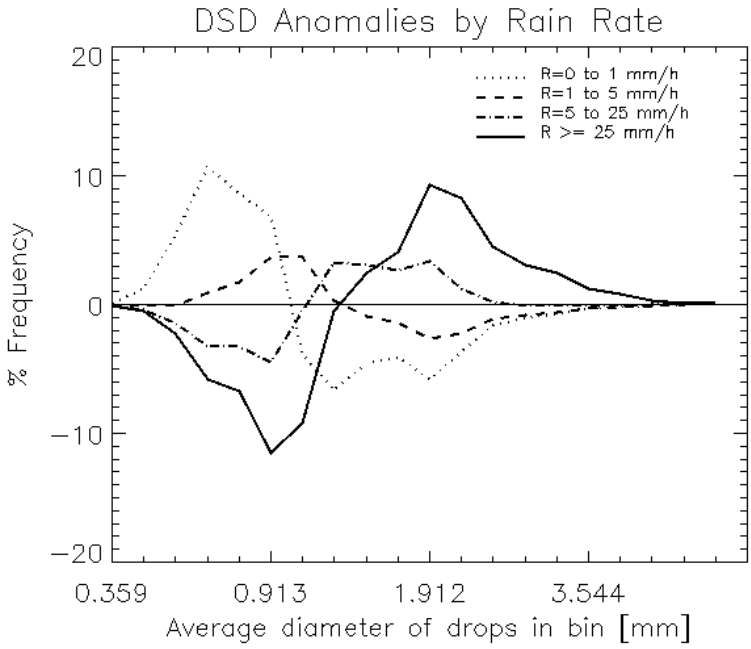

Figure 36 Climatological DSD anomalies by rain rate.

The drop-size distribution anomaly for barotropic storms is analyzed by rain rate (Fig. 37a). R3 is primarily responsible for the positive DSD anomaly in the medium and large drop modes, and the deficiency of small drops. The varying distributions across all rain rates in the medium drop range account for the relatively neutral values in the total DSD anomaly. The strongest convection, represented by R4, has fewer large drops than other baroclinicity regimes (except in the very largest of drop-sizes). The largest negative anomaly of the R2-R3 range across all the baroclinicity regimes is found in the small drop mode of the barotropic distribution, indicating that these stronger rain rates are not the result of an abundance of smaller drops.

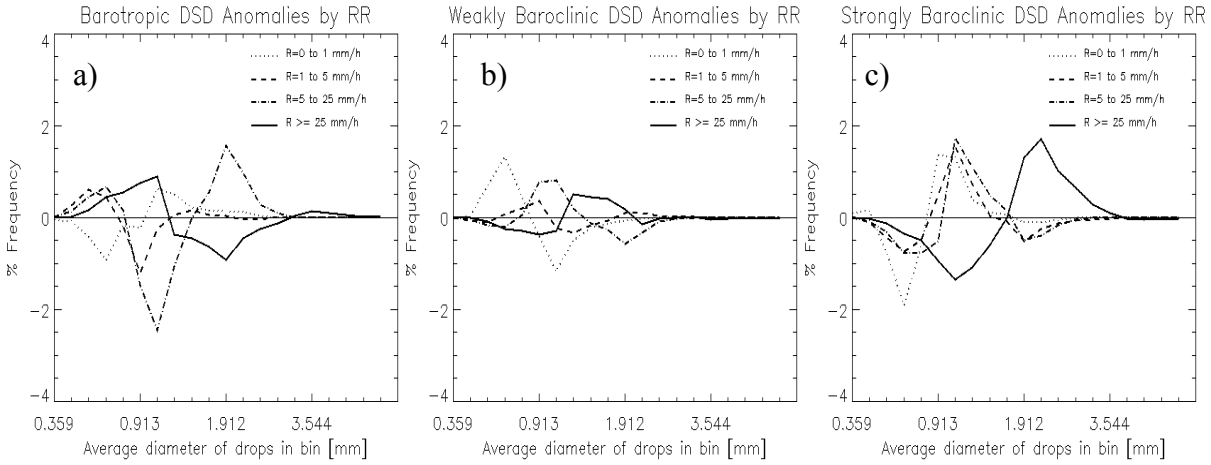

Figure 37 DSD anomalies by rain rate for a) barotropic b) weakly baroclinic and c) strongly baroclinic regimes.

The weakly baroclinic DSD anomalies separated by rain rate distributions are more moderate than in the other regimes, suggesting that the rain rates from conflicting storm types smooth out the weakly baroclinic distribution (Fig. 37b). The distributions of rain rates R1-R3 all have largest peaks in the small drop modes, although at different diameters, suggesting that the weak to moderate convection consists of a large amount of small drops. In contrast, the strongest convection has the most moderate drops, most likely formed in moderate to strong updrafts or stratiform regions.

The strongly baroclinic rain rates are dominated by a combined excess of small drops across all but the strongest rain rates, as well as a combined negative anomaly in the medium to large drop modes (Fig. 37c). The strongest convection, represented by rain rate R4, has the highest amounts of medium to large drops, suggesting that the deep convection and robust stratiform regions are accompanied by strong rain rates.

3.3.7. Comparison of Rainfall Parameters

Table 6 contains a summary of rainfall parameters for both baroclinicity regimes and storm types (Z-R parameters will be discussed separately). The storm averaged rain rates and drop sizes are directly proportional, decreasing from the largest values in the barotropic regime, to the smallest values in the strongly baroclinic regime. The shift in average drops size is consistent with the DSD anomalies by baroclinicity discussed in Section 3.3.3. However, the relationship between R and D_0 is not strictly linear by storm type. The smallest average rain rates are found in warm fronts and upper level disturbances (2.1 and 2.4 mm h^{-1}, respectively), which also have the lowest average drop sizes. The highest average rain rates are from drylines (5.7 mm h^{-1}) with moderate average drop sizes followed by stationary fronts (5.2 mm h^{-1}), which have the highest average drop sizes.

Table 6 Storm averaged rainfall parameters for baroclinicity regimes and storm types.

	R [mm h^{-1}]	**D_0 [mm]**
Barotropic	4.6	1.13
Weakly Baroclinic	3.9	1.11
Strongly Baroclinic	2.6	1.06
Type 1	3.8	1.08
Type 2	5.7	1.12
Type 3	4.0	1.16
Type 4	2.1	0.99
Type 5	5.2	1.21
Type 6	2.4	1.05
All Storms	3.7	1.11

Comparing N_0 values at a constant rain rate for different drop-size distributions can be used to determine whether the precipitation is more convective or stratiform. For

rain rates that can be either convective or stratiform, a higher N_0 indicates that the precipitation has a higher convective fraction (see Section 1.3.4.). Table 7 includes N_0 values for the climatological baroclinicity DSDs for the four rain rate intervals.

Table 7 N_0 values for baroclinicity DSDs at rain rate intervals R1-4.

	B	**W**	**S**
R1	407	534	487
R2	1498	1578	1467
R3	2634	3080	2966
R4	3779	3875	4153

For weak to moderate rain rates, R1-3, weakly baroclinic storms have the highest convective fraction. The convection in the weakly baroclinic regime is weak and composed of many small drops since the peak in the DSD anomaly at these rain rates is in the small drop mode (Fig. 38). At the heaviest rain rates, R4, the strongly baroclinic DSD has the highest convective fraction, with a peak in the medium drop mode. The barotropic regime has the highest stratiform fraction at all rain rates except R2, where the strongly baroclinic regime has more stratiform.

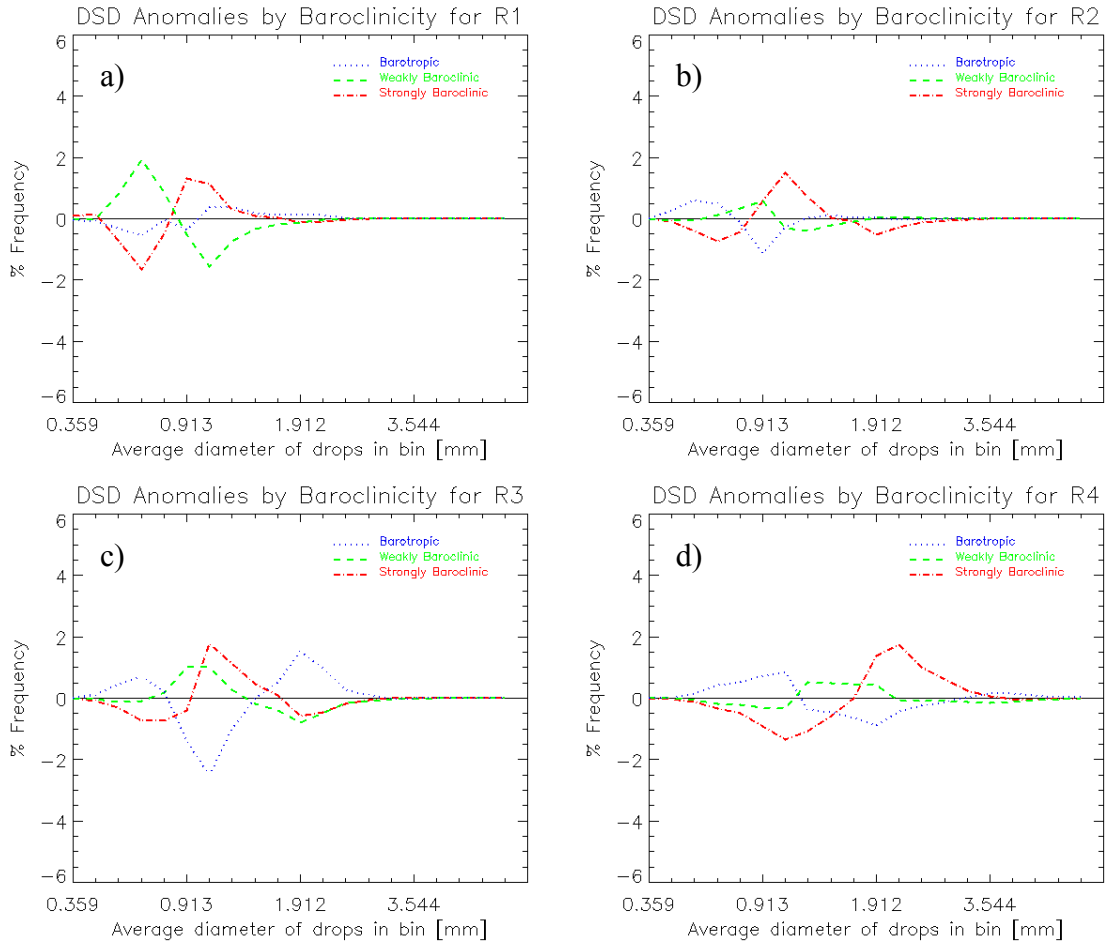

Figure 38 DSD anomalies by baroclinicity for rain rate ranges a) R1 b) R2 c) R3 and d) R4.

A similar separation was made by storm type (Table 8). The highest stratiform fractions are found in the stationary and cold frontal storm types across all rain rates, which is reflected in the high occurrence of medium to large drops in the type 3 and type 5 DSDs. The highest convective fractions are found in the warm frontal and dryline cases, which are primarily composed of small drops. However, for the warm fronts, the drops contributing to the R4 rain rates are actually in the medium drop mode.

Table 8 N_0 values for storm type DSDs at rain rate intervals R1-4

	Type 1	**Type 2**	**Type 3**	**Type 4**	**Type 5**	**Type 6**
R1	485	563	324	677	527	486
R2	1721	2084	1185	2167	1050	1564
R3	3011	3870	2563	3720	1741	3185
R4	4079	4200	3862	4157	3238	4148

Z-R relationships were derived for each of the storms identified from the disdrometer observations. The exponent in the Z-R relationship, *b*, was calculated for each individual storm across the baroclinicity categories (Fig. 39a). Although there is a large spread within each designation, the mean exponent across all storms is 1.327 with less than 1% variation between baroclinicity categories. Since there is little variation in the means, the multiplicative factor, *a*, was calculated using the fixed exponent of 1.327. The resulting mean values show more variation than the exponents, varying by 5% (Fig. 39b). Additionally, the median multiplicative factors across the baroclinicity designations vary by approximately 10%.

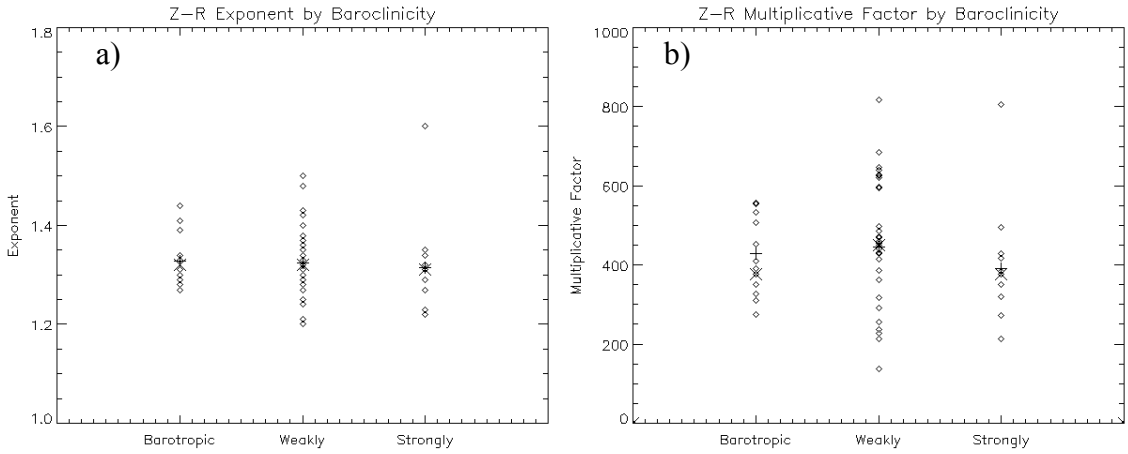

Figure 39 Distribution by baroclinicity of individual storm a) Z-R exponent b) multiplicative factor.

In order to visualize the effects of the Z-R parameters on rainfall calculations between the different regimes, Table 9 compares the rain rates expected at fixed *b*=1.327 for the values derived from the climatology. For a fixed exponent at a specified reflectivity, a higher value for the multiplicative factor results in a lower rain rate. The strongly baroclinic storms would therefore have the highest rain rates and barotropic would have the lowest rain rate with the same observed reflectivity.

Table 9 Rain rates (mm h^{-1}) derived from Z-R relationships at a fixed reflectivity of 40 dBZ.

	a	***b***	**R (40 dBZ) [mm h^{-1}]**
B	443	1.327	10.4
W	412	1.327	11.1
S	394	1.327	11.4

The climatological Z-R relationship calculated from the cumulative DSD for the entire two year period is $Z=425R^{1.32}$. When comparing individual storm Z-Rs there is a

wide variation in values, however the overall average for the storms is $Z=413R^{1.327}$. If the multiplicative factor for each storm is instead calculated using a fixed exponent of 1.327, the result is $Z=431R^{1.327}$. Since there is little difference between all these values, a Z-R relationship of $Z=425R^{1.32}$ reasonably represents the observations. The calculation of climatological Z-R relationships from the DSDs for each baroclinicity regime is found in Table 10. Comparing these results to values reported in Rosenfeld and Ulbrich (2003), our observations have the closest match to those for an Oklahoma thunderstorm, $Z=316R^{1.36}$ and a Congo squall line, $Z=425R^{1.29}$. Translating the baroclinicity designations into different geographical locations around the world would be an interesting project for future study.

Table 10 Climatological Z-R relationships and rain rates at fixed reflectivities of 40 and 50dBZ.

	a	***b***	**R (40 dBZ)**	**R (50 dBZ)**
All Storms	425	1.32	10.9	62.6
Barotropic	456	1.32	10.4	59.4
Weakly Baroclinic	410	1.33	11.0	62.4
Strongly Baroclinic	413	1.31	11.4	66.1
OK Thunderstorm	316	1.36	12.7	68.9
Congo Squall Line	425	1.29	11.6	68.8
Marshall-Palmer	200	1.6	11.5	48.6
NEXRAD	300	1.4	12.2	63.4
NEXRAD Tropical	250	1.2	21.6	147.4

Standard Z-R relationships (i.e., NEXRAD and Marshall-Palmer) are compared to the storm type Z-R relationships at a fixed reflectivity of 50 dBZ using the percent difference between the storm type rain rate derived from the observed Z-R relationship and the estimated rain rate using one of the other Z-R relationships (Table 11). For all

storm types (except type 5b), the best estimate of rain rate would be given by one of the climatological baroclinicity Z-R relationships. However, the application of the total climatological Z-R relationship to the storm types would be more useful operationally since does not require the synoptic and radar data necessary to make the storm type identification.

The performance of the climatological, NEXRAD and Marshall-Palmer Z-R relationships is therefore analyzed (Table 11). The rain rates for non-frontal storm types (1, 2 and 6) are best approximated by the climatological value. NEXRAD performs best for warm fronts, LLTS cold fronts (type 3b) and stationary fronts, and actually gives a better estimate of rain rate at 50 dBZ for type 5b storms than the climatological Z-R. However, the NEXRAD Z-R relationship tends to underestimate the rain rate at 50 dBZ, which has implications for flood prediction. The Z-R relationship derived from the Marshall-Palmer drop-size distribution provides the best estimate for storm types 3a and 3c, which tend to have weaker convection and stratiform precipitation than in the LLTS type 3b storms. Since no single Z-R relationship adequately describes the microphysical processes for the major storm types, multiple Z-R relationships might be useful.

Table 11 Comparison of Z-R relationships by storm type at a fixed reflectivity of 50 dBZ using the percent difference between the storm type rain rate derived from the observed Z-R relationship and the estimated rain rate using Z-R relationships by baroclinicity, total climatology, NEXRAD and Marshall-Palmer (from Table 10). Negative (positive) numbers indicate an underestimation (overestimation) of rain rates compared to the observed storm type. Shading indicates best match with each storm type rain rate.

	R (50 BZ)	B (% Dif)	W (% Dif)	S (% Dif)	All (% Dif)	NEXRAD (% Dif)	M-P (% Dif)
Type 1	58.8	1.0	5.7	11.0	6.1	7.3	-20.9
Type 1a	56.8	4.3	8.9	14.0	9.2	10.4	-16.9
Type 1b	58.7	1.1	5.9	11.2	6.3	7.4	-20.7
Type 2	62.2	-4.7	0.3	5.9	0.7	1.9	-27.9
Type 3	59.7	-0.5	4.3	9.7	4.7	5.9	-22.7
Type 3a	48.1	18.9	33.8	27.1	23.1	24.1	1.0
Type 3b	76.3	-28.5	-22.3	-15.5	-21.8	-20.3	-56.9
Type 3c	53.3	10.3	14.6	19.4	14.9	16.0	-9.5
Type 4	87.0	-46.6	-39.5	-31.7	-39.0	-37.2	-79.0
Type 5	65.7	-10.6	-5.3	0.6	-4.9	-3.6	-35.1
Type 5a	73.0	-22.9	-17.0	-10.5	-16.5	-15.1	-50.1
Type 5b	63.3	-6.6	-1.5	4.2	-1.1	0.2	-30.2
Type 6	61.8	-4.2	0.8	6.4	1.2	2.5	-27.2

4. CONCLUSIONS

A two-year climatology of baroclinicity designations, storm type and drop-size distributions over Southeast Texas was collected from December 2004 through November 2006. Three baroclinicity designations – barotropic, weakly baroclinic and strongly baroclinic – were identified using horizontal temperature differences and vertical wind shear from NCEP data. Precipitating systems were grouped by dynamical forcing and precipitation structure into the six dynamical categories and structure subcategories that are used to identify the storm type. The drop-size distributions collected by the JW disdrometer were used to identify storms during the observation period and analyzed for patterns by baroclinicity and storm type. The mechanisms forming the droplets within the precipitating systems differ by type of storm and baroclinicity regime. Thus, these long-term climatologies identify patterns that can be used to interpret new data and link microphysical processes to storm organization and large-scale forcing.

The barotropic environment is characterized by a lack of strong temperature differences and vertical wind shear and occurs most frequently in summer. Typical barotropic storms are associated with weak forcing (type 1), drylines (type 2) and upper level disturbances (type 6). The climatological barotropic DSD is weighted strongly towards medium to large drops, reflecting moderate to strong convection accompanied by stratiform precipitation. The highest storm average drop-sizes and rain rates are found in the barotropic regime, which is consistent with the DSD anomalies.

The weakly baroclinic environment is characterized by moderate temperature differences and wind shear, occurring most frequently in winter followed by spring and fall. Storm types across all dynamic forcings are possible in weakly baroclinic environments, but cold and stationary fronts develop most often (particularly types 3c and 5b). The resulting DSD anomalies are small due to the conflicting microphysical processes in different storm types. The weak convection in storm types 2, 4 and 6 is weighted more towards small drops, whereas the stronger convection and stratiform precipitation from type 3 and 5 storms are weighted towards larger drops. Weakly baroclinic storms have more moderate rain rates resulting from many small to medium drops.

The strongly baroclinic environment is characterized by the strongest temperature differences and vertical wind shear, which are present most frequently in winter. Cold fronts are the most common storm type in the strongly baroclinic environment, followed by warm fronts and upper level disturbances. The climatological strongly baroclinic DSD is heavily weighted towards small drops, which are associated with the weaker convection in strongly baroclinic type 4, 5 and 6 storms. The weak convection leads to the smallest average rain rates and storm average drop-sizes.

Non-frontal storm types (i.e., storms associated with weak forcing, drylines and upper level disturbances) occur most frequently in barotropic environments, although type 6 storms have a tendency towards stronger wind shear. The DSDs for types 1, 2 and 6 are all weighted towards smaller drops, but barotropic type 2 storms are weighted towards larger drops compared to the weakly baroclinic regime. While weak convection

dominates the DSDs, stronger convection and stratiform precipitation are also possible, particularly in storm types 1b and 2. The climatological Z-R relationship of $Z=425R^{1.32}$ is a better approximation of non-frontal rain rates in SE Texas than the NEXRAD and Marshall-Palmer.

Frontal storm types (i.e., storms associated with cold, stationary and warm fronts) occur primarily in weakly and strongly baroclinic environments. Types 3a/b show a tendency towards stronger temperature differences, while types 4 and 5b have a predisposition towards stronger wind shear. The DSD in warm frontal storms is distinctly different from the DSD in cold and stationary fronts. While warm fronts are heavily weighted towards small drops from widespread weak convection, the cold and stationary fronts (particularly 3b and 5b) are weighted towards larger drops from the deep convection and stratiform precipitation of MCSs and LLTS storms. Storm types 3 and 5 have a lower convective to stratiform ratio than type 4, which has more convection that is particularly evident in the small drop mode. The differences between the frontal types suggest that warm fronts should not be combined with the cold/stationary fronts because the microphysical processes are distinctly different.

A longer-term climatology and future radar analysis will help to isolate the microphysical properties of the storm types and the manner in which the baroclinicity of the environment modifies the precipitation. Performing a similar study at different geographical locations in the subtropics could ascertain whether the baroclinicity designations can be applied on a broader scale or if they are particular to SE Texas.

REFERENCES

Atlas, D., 1990: *Radar in Meteorology*, American Meteorological Society, 806 pp.

Byers, H.R., and R.R. Braham, 1949: *The Thunderstorm*. U.S. Gov. Printing Office, Washington, DC, 287 pages.

Cook, K.H., 2003: Role of continents in driving the Hadley cells. *J. Atmos. Sci.*, **60**, 957-976.

Duchon C. E., and G. R. Essenberg, 2001: Comparative rainfall observations from pit and aboveground rain gauges with and without wind shields. *Water. Resour. Res.*, **37**, 3253–3263.

Dye, J. E., C. A. Knight, V. Toutenhoofd, and T. W. Cannon, 1974: The mechanism of precipitation formation in northeastern Colorado cumulus. III. Coordinated microphysical and radar observations and summary. *J. Atmos. Sci.,* **31,** 2152–2159.

Encyclopedia of Earth (June 2007): Mid-latitude cyclone. http://www.eoearth.org/article/Mid-latitude_cyclone.

Habib E., W. F. Krajewski, and A. Kruger, 2001: Sampling errors of tipping-bucket rain gauge measurements. *J. Hydrol. Eng.*, **6**, 159–166.

Hobbs, P. V., T. J. Matejka, P. H. Herzegh, J. D. Locatelli, and R. A. Houze Jr., 1980: The mesoscale and microscale structure and organization of clouds and precipitation in midlatitude cyclones. I: A case study of a cold front. *J. Atmos. Sci.*, **37,** 568–596.

Holton, J. R., 1992: *An Introduction to Dynamic Meteorology*. Academic Press, 511 pp.

Hou, A. Y., 1998: Hadley circulation as a modulator of the extratropical climate. *J. Atmos. Sci.*, **55**, 2437–2457.

Houghton, H. G., 1968: On precipitation mechanisms and their artificial modification. *J. Appl. Meteorol.*, **7**, 851-859.

Houze, R. A., Jr., 1977: Structure and dynamics of a tropical squall-line system. *Mon. Weather Rev*., **105**, 1540–1567.

_____, 1993: *Cloud Dynamics*. Academic Press, 573 pp.

_____, 1997: Stratiform precipitation in regions of convection: A meteorological paradox? *Bull. Am. Meteorol. Soc*., **78**, 2179–2196.

_____, 2004: Mesoscale convective systems. *Rev. Geophys*, **42**, 43 pp.

_____, and A. K. Betts, 1981: Convection in GATE. *Rev. Geophys*., **19**, 541–576.

_____, S. A. Rutledge, M. I. Biggerstaff, and B. F. Smull, 1989: Interpretation of Doppler weather-radar displays in midlatitude mesoscale convective systems. *Bull. Am. Meteorol. Soc.* **70**, 608–619.

Jameson, A. R. and A. B. Kostinski, 2001: What is a raindrop-size distribution? *Bull. Am. Meteorol. Soc.,* **82**, 1169-1177.

Joss, J. and A. Waldvogel, 1967: Ein Spektrograph für Niederschlagstropfen mit automatischer Auswertung (A spectrograph for rain drops with automatical analysis). *Pure Appl. Geophys.,* **68,** 240–246.

_____, and _____, 1969: Raindrop-size Distribution and Sampling Size Errors. *J. Atmos. Sci.*, **26**, 566–569.

List R. and G. M. McFarquhar, 1990: The role of breakup and coalescence in the three-peak equilibrium distribution of raindrops. *J. Atmos. Sci.*, **47**, 2274–2292.

Marshall, J. S. and W. McK. Palmer, 1948: The distribution of raindrops with size. *J. Atmos. Sci.*, **5**, 165-166.

Matejka, T. J., R. A. Houze Jr., and P. V. Hobbs, 1980: Microphysics and dynamics of clouds associated with mesoscale rainbands in extratropical cyclones. *Quart. J. Roy. Meteor. Soc.,* **106,** 29–56.

McFarquhar, G. M. and R. List, 1993: The effect of curve fits for the disdrometer calibration on raindrop spectra, rainfall rate, and radar reflectivity. *J. Appl. Meteor.*, **32**, 774–782.

_____, 2004: A new representation of collision-induced breakup of raindrops and its implications for the shapes of raindrop-size distributions. *J. Atmos. Sci.*, **61**, 777–794.

Nesbitt, S.W., and E.J. Zipser, 2003: The diurnal cycle of rainfall and convective intensity according to three years of TRMM measurements. *J. Climate*, **16**, 1456-1475.

Rosenfeld, D. and C. W. Ulbrich, 2003: Cloud microphysical properties, processes, and rainfall estimation opportunities. *Meteorological Monographs*, **52**, 237-258.

Rutledge, S. A., and R. A. Houze, Jr., 1987: A diagnostic modeling study of the trailing stratiform region of a midlatitude squall line. *J. Atmos. Sci.,* **44**, 2640-2656.

Schaefer, J. T., 1974: A simulative model of dryline motion. *J. Atmos. Sci.,* **31,** 956–964.

Schumacher, C., and R. A. Houze Jr., 2003a: The TRMM precipitation radar's view of shallow, isolated rain. *J. Appl. Meteor.*, **42**, 1519-1524.

_____, and _____, 2003b: Stratiform rain in the tropics as seen by the TRMM precipitation radar. *J. Climate*, **16**, 1739–1756.

Seifert, A. 2005: On the shape–slope relation of drop-size distributions in convective rain. *J. Appl. Meteor,* **44,** 1146–1151.

Sempere Torres D., J. M. Porrà, and J.-D. Creutin, 1994: A general formulation for raindrop-size distribution. *J. Appl. Meteor.*, **33**, 1494–1502.

Sheppard, B. E., 1990: Effect of irregularities in the diameter classification of raindrops by the Joss-Waldvogel disdrometer. *J. Atmospheric and Oceanic Tech*., **7,** 180–183.

Smith P. L. Jr., Z. Liu, and J. Joss, 1993: A study of sampling-variability effects in raindrop-size observations. *J. Appl. Meteor.*, **32**, 1259–1269.

Steiner M., and J. A. Smith, 1998: Convective versus stratiform rainfall: An ice-microphysical and kinematic conceptual model. *Atmos. Res.*, **48**, 317–326.

_____, and _____, 2000: Reflectivity rain rate and kinetic energy flux relationships based on raindrop spectra. *J. Appl. Meteor.*, **39**, 1923-1940.

Trenberth, K. E., and D. P. Stepaniak, 2003: Seamless poleward atmospheric energy transports and implications for the Hadley circulation. *J. Climate*, **16**, 3705-3721.

Tokay A., and D. A. Short, 1996: Evidence from tropical raindrop spectra of the origin of rain from stratiform versus convective clouds. *J. Appl. Meteor.*, **35**, 355–371.

_____, D. B. Wolff, K. R. Wolff, and P. Bashor, 2003b: Rain gauge and disdrometer measurements during the Keys Area Microphysics Project (KAMP). *J. Atmos. Oceanic Technol.*, **20**, 1460–1477.

Uijlenhoet, R., J. A. Smith, and M. Steiner, 2003: The microphysical structure of extreme precipitation as inferred from ground-based raindrop spectra. *J. Atmos. Sci.*, **60**, 1220–1238.

Ulbrich, C. W., 1983: Natural variations in the analytical form of the raindrop-size distribution. *J. Appl. Meteor.,* **22,** 1764–1775.

Waldvogel, A., 1974: The N_0 jump of raindrop spectra. *J. Atmos. Sci.*, **31**, 1067-1078.

Wallace, J. M. and P. V. Hobbs, 1977: *Atmospheric Science, An Introductory Survey*. Academic Press, 467 pp.

Zipser, E.J., 2003: Tropical precipitating systems in *Handbook of Weather, Climate, and Water: Dynamics, Climate, Physical Weather Systems, and Measurements*, T. Potter and B. Colman, Ed. John Wiley & Sons, New York, Chapter 30.

APPENDIX A

Table 12 Microphysical parameters from DSD observations during 74 storms from December 2004 through November 2006, including baroclinicity classifications of barotropic (B), weakly baroclinic (W), and strongly baroclinic (S), and storm type designations identified from climatology. Storms 1-3 occurred prior to December 2004.

Storm	Date	Duration [hh:mm]	RA [mm]	Max R [mm h^{-1}]	a	b	Bar.	Storm Type
4	12/22/04	04:55	9.7	51.8	629	1.32	W	3c
5	01/02/05	09:21	20.2	46.8	237	1.33	W	1b
6	01/05/05	01:27	5.5	29.3	137	1.20	W	3a
7	01/13/05	05:59	24.0	75.4	450	1.29	S	3b
8	01/27-28/05	19:40	21.9	32.7	257	1.27	W	4b
9	01/30-31/05	18:39	7.0	33.2	214	1.24	W	4b
10	02/01-02/05	15:12	11.2	10.8	351	1.32	W	5a
11	02/06/07/05	06:02	63.8	52.6	228	1.25	W	2
12	02/23/05	05:36	9.8	42.0	460	1.32	W	5b
13	02/24/05	00:40	3.9	28.7	639	1.35	W	3c
14	02/24/05	06:37	30.0	111.4	497	1.27	W	3b
15	02/26-27/05	15:18	9.6	3.0	363	1.38	S	6
16	03/02/05	07:37	14.3	12.3	431	1.36	W	5b
17	03/07/05	02:33	5.6	39.2	257	1.21	nA	2
18	03/19-20/05	03:35	35.3	77.5	805	1.60	W	5b
19	03/21/05	04:24	9.9	110.4	455	1.34	W	3c
20	03/27/05	05:19	5.3	5.2	404	1.32	nA	6
21	04/01/05	01:35	15.1	79.4	686	1.48	S	3a
22	04/06/05	00:56	21.6	92.6	472	1.31	W	3a
23	05/29/05	03:19	9.5	45.0	335	1.38	W	5b
24	07/08/05	02:59	30.1	110.1	495	1.34	B	2
25	07/09/05	00:38	11.7	64.6	625	1.50	B	1a
26	07/14-15/05	10:44	31.7	59.1	441	1.28	B	2
27	07/15/05	05:12	6.3	19.2	275	1.27	B	6
28	07/16-17/05	07:55	6.9	52.7	376	1.33	W	1b
29	07/17/05	05:25	10.7	94.2	328	1.31	B	1b
30	07/18/05	04:04	3.8	70.2	556	1.41	W	1a
31	08/08-09/05	14:05	3.4	7.0	428	1.33	B	1b
32	08/10/05	05:01	44.6	85.6	411	1.34	B	2
33	08/14/05	01:21	2.3	42.5	684	1.43	B	1b
34	09/10/05	07:17	18.3	116.0	390	1.29	B	1b
35	10/10/05	11:25	20.3	18.1	350	1.33	B	1b
36	10/11/05	05:53	3.7	18.2	311	1.29	W	3c
37	10/31/05	03:37	15.0	75.7	555	1.39	W	3b
38	11/15/05	01:05	10.5	72.2	533	1.28	S	3a

Table 12 Continued

Storm	Date	Duration [hh:mm]	RA [mm]	Max R [mm h^{-1}]	a	b	Bar.	Storm Type
39	11/26/05	03:57	7.2	7.0	452	1.44	S	5b
40	11/28/05	01:08	4.8	22.5	818	1.42	S	3a
41	12/07-08/05	15:18	3.1	5.7	272	1.23	S	3c
42	12/14/05	08:14	7.3	53.3	320	1.31	W	3c
43	01/16-17/06	16:36	5.1	7.1	320	1.22	S	3c
44	01/20-21/06	07:37	3.0	17.2	417	1.35	W	3a
45	01/22/06	19:55	32.2	60.5	317	1.31	S	4b
46	01/28/06	13:54	31.0	68.9	377	1.27	W	3c
47	02/01-02/06	12:00	18.1	64.6	594	1.38	nA	4b
48	02/10/06	06:10	13.8	44.0	214	1.27	S	4a
49	02/25/06	08:04	14.1	23.1	292	1.28	S	6
50	03/20/06	13:10	37.9	116.1	443	1.32	W	6
51	03/28/06	06:26	43.5	48.9	429	1.29	W	5a
52	04/21/06	04:33	25.9	118.9	384	1.34	W	5b
53	04/21/06	01:47	19.1	66.9	485	1.31	W	5b
54	04/29/06	02:50	10.0	113.2	414	1.33	W	3b
55	05/04/06	0:36	10.5	102.0	598	1.40	W	2
56	05/05/06	03:57	3.1	5.0	647	1.37	W	3c
57	05/06/06	03:48	30.3	96.2	470	1.31	W	5b
58	05/08/06	01:50	14.1	75.0	508	1.30	nA	5b
59	05/14/06	02:27	7.7	33.0	620	1.36	W	3c
60	05/31-06/01/06	10:54	7.6	9.0	387	1.30	B	6
61	06/16/06	06:51	12.1	63.1	545	1.34	B	1b
62	06/17/06	09:58	9.5	39.0	297	1.31	B	2
63	06/18/06	02:01	21.7	88.3	340	1.32	B	3b
64	06/21/06	0:27	6.0	61.4	316	1.34	B	1a
65	06/22-23/06	03:15	8.7	101.5	1089	1.44	B	1b
66	07/01-02/06	03:35	10.7	71.8	571	1.33	B	6
67	07/02/06	08:10	6.3	20.8	346	1.31	B	6
68	07/04/06	08:13	13.1	36.2	406	1.29	B	1b
69	07/05/06	16:00	6.5	19.8	312	1.28	B	1b
70	07/24/06	03:14	23.7	68.2	666	1.41	B	5a
71	08/07/06	02:50	14.7	149.3	454	1.36	B	1b
72	08/07-08/06	15:37	14.0	27.2	253	1.25	B	1b
73	09/05/06	08:24	3.2	4.0	301	1.29	W	3c
74	10/18/06	01:59	30.8	130.4	348	1.32	S	3c
75	10/25-26/06	15:04	27.9	38.4	250	1.28	W	6
76	11/06/06	07:23	2.7	37.8	485	1.33	W	3c
77	11/30/06	07:06	6.9	26.7	301	1.23	nA	3c

APPENDIX B

Table 13 Characteristics of twenty drop-size classes used by the DISDRODATA software to process measured RD-80 JW disdrometer measurements, including lower threshold of drop diameter (D_l), average diameter of drops in bin (D_i), fall velocity of a drop with diameter D_i ($v(D_i)$) and diameter interval of drop-size class (ΔD_i).

Class	D_l [mm]	D_i [mm]	$v(D_i)$ [m/s]	ΔD_i [mm]
1	0.313	0.359	1.435	0.092
2	0.405	0.455	1.862	0.100
3	0.505	0.551	2.267	0.091
4	0.596	0.656	2.692	0.119
5	0.715	0.771	3.154	0.112
6	0.827	0.913	3.717	0.172
7	0.999	1.116	4.382	0.233
8	1.232	1.331	4.986	0.197
9	1.429	1.506	5.423	0.153
10	1.582	1.665	5.793	0.166
11	1.748	1.912	6.315	0.329
12	2.077	2.259	7.009	0.364
13	2.441	2.584	7.546	0.286
14	2.727	2.869	7.903	0.284
15	3.011	3.198	8.258	0.374
16	3.385	3.544	8.556	0.319
17	3.704	3.916	8.784	0.423
18	4.127	4.350	8.965	0.446
19	4.573	4.859	9.076	0.572
20	5.145	5.373	9.137	0.455

VITA

Name:	Karen Elizabeth Brugman
Address:	Department of Atmospheric Sciences, Texas A&M University, 3150 TAMU, College Station, TX 77843-3150
Email Address:	kbrugman@tamu.edu
Education:	B.S., Atmospheric, Oceanic and Environmental Sciences, University of California, Los Angeles, 2001 M.S., Atmospheric Sciences, Texas A&M University, 2007